AFRL-RX-WP-TP-2011-4299

OBSERVATIONS ON THE ROLE OF HYDROGEN IN FACET FORMATION IN NEAR-α TITANIUM (Preprint)

A.L. Pilchak

Processing Section
Metals Branch

J.C. Williams

Universal Technology Corporation

MAY 2011

AIR FORCE RESEARCH LABORATORY
MATERIALS AND MANUFACTURING DIRECTORATE
WRIGHT-PATTERSON AIR FORCE BASE, OH 45433-7750
AIR FORCE MATERIEL COMMAND
UNITED STATES AIR FORCE

REPORT DOCUMENTATION PAGE

Form Approved
OMB No. 0704-0188

1. REPORT DATE *(DD-MM-YY)*	2. REPORT TYPE	3. DATES COVERED *(From - To)*
May 2011	Journal Article Preprint	01 May 2011 – 01 May 2011

4. TITLE AND SUBTITLE
OBSERVATIONS ON THE ROLE OF HYDROGEN IN FACET FORMATION IN NEAR-α TITANIUM (Preprint)

5a. CONTRACT NUMBER
In-House

5b. GRANT NUMBER

5c. PROGRAM ELEMENT NUMBER
62102F

6. AUTHOR(S)
A.L. Pilchak (Metals Branch, Processing Section (AFRL/RXLMP))
J.C. Williams (Universal Technology Corporation)

5d. PROJECT NUMBER
4347

5e. TASK NUMBER
20

5f. WORK UNIT NUMBER
25100102

7. PERFORMING ORGANIZATION NAME(S) AND ADDRESS(ES)

Metals Branch, Processing Section (AFRL/RXLMP)
Materials and Manufacturing Directorate, Metals, Ceramics, and NDE Division
Air Force Research Laboratory
Wright-Patterson Air Force Base, OH 45433-7750
Air Force Materiel Command, United States Air Force

Universal Technology Corporation

8. PERFORMING ORGANIZATION REPORT NUMBER
AFRL-RX-WP-TP-2011-4299

9. SPONSORING/MONITORING AGENCY NAME(S) AND ADDRESS(ES)

Air Force Research Laboratory
Materials and Manufacturing Directorate
Wright-Patterson Air Force Base, OH 45433-7750
Air Force Materiel Command
United States Air Force

10. SPONSORING/MONITORING AGENCY ACRONYM(S)
AFRL/RXLM

11. SPONSORING/MONITORING AGENCY REPORT NUMBER(S)
AFRL-RX-WP-TP-2011-4299

12. DISTRIBUTION/AVAILABILITY STATEMENT
Approved for public release; distribution unlimited.

13. SUPPLEMENTARY NOTES
PAO case number 88ABW-2010-3852, cleared 16 July 2010. The U.S. Government is joint author of this work and has the right to use, modify, reproduce, release, perform, display, or disclose the work. Submitted to Metallurgical and Materials Transactions A. Document contains color.

14. ABSTRACT
Faceted features are frequently observed on the fracture surfaces of titanium alloys that have failed by static loading, continuous cycling, dwell fatigue loading, and stress corrosion cracking. Although the facets formed under different loading conditions appear qualitatively similar, there are significant differences in the spatial and crystallographic orientations of the facets as well as subtle differences in facet surface topography. The present study compares and contrasts facets in the Ti-8Al-1Mo-1V alloy with the primary motivation being to understand the mechanisms of crack initiation and faceted growth during dwell fatigue. The spatial and crystallographic orientations of the facets were determined using quantitative tilt fractography and electron backscatter diffraction while facet topography was examined using ultra high resolution scanning electron microscopy. Collectively, these observations suggest that hydrogen plays an important role in facet formation and accelerating small crack growth rates during dwell fatigue loading.

15. SUBJECT TERMS
facet, static loading, dwell fatigue, cycling

16. SECURITY CLASSIFICATION OF:			17. LIMITATION OF ABSTRACT:	18. NUMBER OF PAGES	19a. NAME OF RESPONSIBLE PERSON (Monitor)
a. REPORT	b. ABSTRACT	c. THIS PAGE			Donna Ballard
Unclassified	Unclassified	Unclassified	SAR	76	19b. TELEPHONE NUMBER *(Include Area Code)* N/A

Observations on the role of hydrogen in facet formation in near-α titanium

A.L. Pilchak[1,2,3] and J.C. Williams[1]

[1] The Ohio State University, Department of Materials Science and Engineering, Columbus OH 43210

[2] Air Force Research Laboratory, Materials and Manufacturing Directorate, RXLMP
Wright Patterson Air Force Base OH 45433

[3] Universal Technology Corporation, Dayton OH 45432

Abstract

Faceted features are frequently observed on the fracture surfaces of titanium alloys that have failed by static loading, continuous cycling, dwell fatigue loading and stress corrosion cracking. Although the facets formed under different loading conditions appear qualitatively similar, there are significant differences in the spatial and crystallographic orientations of the facets as well as subtle differences in facet surface topography. The present study compares and contrasts facets in the Ti-8Al-1Mo-1V alloy with the primary motivation being to understand the mechanisms of crack initiation and faceted growth during dwell fatigue. The spatial and crystallographic orientations of the facets were determined using quantitative tilt fractography and electron backscatter diffraction while facet topography was examined using ultra high resolution scanning electron microscopy. Collectively, these observations suggest that hydrogen plays an important role in facet formation and accelerating small crack growth rates during dwell fatigue loading.

I. Introduction

Based on a number of experimental observations over the past several decades, there is a basic understanding of the sequence of crack formation during continuous cycling. A number of researchers have observed first the formation of planar slip bands, followed by crack initiation and propagation along these slip bands [1-3]. On the fracture surface, cracking along a slip band leads to the formation of planar features that are commonly referred to as facets [4]. In addition to being present on failures resulting from continuous cycling, facets are also characteristic of the fracture surfaces near the origin areas of specimens that have failed by dwell fatigue [5-7], static loading in air [8,9] and stress corrosion cracking [10,11]. Among these, there has been considerable controversy surrounding the origins and characteristics of facets found on dwell fatigue specimens.

Dwell fatigue failures created in the laboratory and occurring in service are generally characterized as having subsurface crack initiation sites with planar facets that can be either inclined or nearly perpendicular to the loading direction depending on the magnitude of applied stress [6,8,12]. Furthermore, dwell fatigue facets have been widely generalized as being “on or near” the basal plane [6,12-15]. Early work by Evans [12] suggested that the facet planes were oriented within 5^{o} of the basal plane, and were also nearly perpendicular to the loading direction. Thus, it became necessary to rationalize how slip could occur on basal planes that were oriented nearly perpendicular to the loading direction that had essentially zero resolved shear stress. Later, Evans and Bache [6] proposed a conceptual model based on Stroh’s formulation of the stress field around a dislocation pileup in an isotropic material and subsequent crack nucleation from this pileup. This model is shown schematically in Figure 1.

The authors contended that at low applied stress levels only the most suitably oriented grains with slip planes inclined to the loading direction would be able to accumulate strain by dislocation slip (the “soft

grain"). The so-called source slip band is blocked by a grain boundary such that a dislocation pileup forms. The dislocation pileup that forms on the source slip band induces a normal stress and a shear stress field that is resolved onto the basal plane of the adjacent grain (the "hard grain"). The magnitude of the resolved stress depends primarily on the angle between the source slip band and the slip plane in the adjacent grain as well as the available slip length (which determines the maximum pileup length) in the soft grain. In the Evans and Bache [6] adaptation of Stroh's original model, it was suggested that the shear stress induced by the pileup in the soft grain provided sufficient shear stress onto the basal plane of the hard grain such that slip could occur. Additionally, the resolved normal stress would combine with the far field applied stress to cause decohesion of the slip band on the (0001) plane of the hard grain resulting in facet formation along the slip band.

The Stroh-like model proposed by Evans and Bache [6], while conceptually useful for understanding some experimental observations, does not explain the time dependent nature of dwell fatigue, nor incorporate the anisotropic elasticity or plasticity of the α phase. The model is based on the assumption that slip is required prior to crack initiation and assumes that the crack initiates on the basal plane of the hard grain which is orthogonal to the loading direction. The requirement that slip precedes facet formation, however, has not been experimentally demonstrated satisfactorily. In addition, there was evidence as early as 1980 [16] that dwell facet fracture planes were not coincident with the basal plane. Davidson and Eylon [16] used selected area electron channeling to determine the crystallographic plane of fracture to an accuracy of +/- 3^{o} on dwell facets of continuously cycled and dwell fatigued IMI-685. The authors also made a distinction between those facets near the crack initiation site and those which were propagation facets. In both locations on the dwell fatigued specimen, the facet planes were consistently oriented between 5^{o} and 15^{o} from the basal plane, with the larger angular deviations being preferred over the smaller ones in the propagation facet regime. In contrast, the facets on specimens subjected to continuous cycling fractured

considerably nearer the basal plane. The initiation facets were reported to be precisely on the basal plane while the propagation facets showed deviations as large as 10^{o} from it. However, the angle between the facet normal direction and the loading direction was not explicitly reported for each facet.

Sinha et al. [7,8] have recently supported these measurements using a higher fidelity combined tilt fractography / electron backscatter diffraction (EBSD) technique in which both the crystallographic orientation of the fractured grain and the spatial orientation of the facet are considered for an accurate determination of facet crystallography. Sinha et al. [7,8] examined only propagation facets on specimens of Ti-6242 subjected to continuous cycling, static loading in air and 2 minute dwell fatigue cycles. The fracture planes of the dwell and continuously cycled specimen were consistent with those observed by Davidson and Eylon [16], being inclined to (0001) approximately 5^{o} and 10^{o} ~ 15^{o}, respectively. In addition, the analysis by Sinha et al. [8] showed that the fracture plane of facets formed during static loading deviated approximately 15^{o} ~ 20^{o} from (0001). More recently, Uta et al. [17] have also reported deviations between 10^{o} and 20^{o} from the basal plane on dwell fatigue crack propagation facets in IMI834 after accounting for their spatial orientation. In contrast, the authors reported that the initiation facets on dwell fatigue specimens were more nearly coincident with the basal plane. Unfortunately, the spatial orientations were not explicitly reported for the initiation or propagation facets.

In the present study, we have analyzed the spatial and crystallographic orientations of initiation and propagation facets formed by continuous cycling, static loading both in air and in 3.5 pct. NaCl and by dwell fatigue loading. In addition to studying the crystallographic and spatial orientations, we have also used ultra high resolution scanning electron microscopy to study the surface topography of the facets in order to utilize it along with the crystallographic information to further understand the micromechanisms of crack initiation and propagation during dwell fatigue.

II. Materials and experimental procedure

A 12.7 cm diameter, 127 cm long Ti-8Al-1Mo-1V bar was provided by Timet (Henderson, NV). Blanks for mechanical test specimens were extracted transverse to the bar axis by wire electrical discharge machining. All of the tests were performed on material in the as-received condition. The blanks were machined into round specimens with one of the two geometries shown in Figure 2. The specimens were tested under four different loading conditions, continuous cycling at 30 Hz, 2 min dwell periods with 1 second each down- and up-ramp loading, static loading at room temperature in lab air and static loading in 3.5 pct. NaCl. All of the tests were run in load control and the peak stress attained during any one test was constant for all tests at 758 MPa, which was 95 pct. of the yield strength measured from a tensile test conducted according to ASTM E8 standards. The load ratio was 0.1 for the continuous cycling and dwell tests. The cyclic tests were performed on a servohydraulic test frame that had been precisely aligned with a strain gauged standard specimen prior to testing. The stress corrosion and static loading experiments were performed on an M-Cert Test System (InterCorr International, Inc., Houston, Texas) which is controlled by a precision step-motor. Since Ti-811 exhibits increased susceptibility to stress corrosion cracking in 3.5 pct. NaCl in the presence of a notch [18], a diamond scribe was used to arbitrarily scratch 1 mm to 2 mm lines around the circumference of the gauge section in several random locations perpendicular to the loading direction.

The microstructural characterization and fractographic investigations were performed with a FEI (FEI Company, Hillsboro, OR) Sirion field emission gun (FEG) scanning electron microscope (SEM) while quantitative tilt fractography and EBSD measurements were performed in either an FEI Quanta 200 tungsten emission source SEM or an FEI XL30 FEG SEM. For imaging purposes, a 30 μm objective aperture was utilized with accelerating voltages varying between 12 kV and 20 kV and spot sizes of either 4 or 5. Images were acquired using the secondary electron detector as well as the through-lens detector

(TLD) when the Sirion was operated in ultra-high resolution (UHR) mode. The TLD is a scintillation detector that is mounted inside the pole piece of the SEM. In this configuration, the electrons used to create the image must pass through the pole piece to return to the detector so only the highest energy electrons are collected. This detector can be either positively or negatively biased to collect secondary or backscattered electrons, respectively. A positive bias of 20 V was utilized in the present study. In addition, selecting this imaging mode alters the magnetic field in the SEM chamber which refines the probe size, thereby increasing the resolution of the SEM. In contrast, a larger probe size is desired for the tilt fractography experiments, so a 100 μm objective aperture was used in conjunction with a 20 kV accelerating voltage to produce a high beam current, on the order of 10 nA, in order to provide as large of a backscattered volume as possible to penetrate surface layers of plastically deformed material. Even under these conditions, the interrogated volume is still very small compared to the grain size and so each pattern collected originates from a single grain.

A. Spatial orientation and the crystallographic plane of fracture

The technique to fully characterize the faceted initiation sites by determining both the spatial orientation of the facet and the crystallographic plane of fracture has been described previously [4,7,8,19]. In brief, the technique involves acquiring images of the same location at two different tilt angles and identifying a common origin and three common features in both images. The coordinates of each feature is then determined within a fixed image coordinate system that is chosen to coincide with the reference frame of the EBSD system being utilized. Using the equations developed by Themelis et al. [20], the spatial orientation of the facet are used to determine two vectors that lie in the plane of the facet whose cross product defines a unit vector within the sample reference frame that defines the facet normal. An inverse pole figure centered on the facet normal vector containing the orientation of the faceted grain as-measured by EBSD is calculated to determine the crystallographic plane of fracture. Recently, we have also shown

that calculating an inverse pole figure with respect to the vectors in the facet plane can also be useful to correlate the local dominant crack growth direction with crystallographic orientation if the vectors are strategically placed in the plane of the facet [4].This technique is reported to be accurate between 1^o [8] and 3^o [21] when the spatial and crystallographic information is collected in the same microscope session without rotating the stage. Thus, in the present work, we have rounded the spatial orientations of the facets with respect to the loading axis to the nearest integer.

III. Results and discussion

A. Characterization of as-received bar

The microstructure (Figure 3) and microtexture (Figure 4) of the as-received bar was characterized with scanning electron microscopy and EBSD methods. The bi-modal microstructure consisted of a globular α grains approximately 10 μm to 15 μm in diameter. The secondary α, on the other hand, was not arranged into well-defined colonies as in classical bi-modal microstructures. Instead, the secondary α, which accounted for approximately 30 vol. pct. to 35 vol. pct. of the microstructure, was relatively coarse and in many locations appeared to have multiple variants of α phase. EBSD analysis has shown that, in many locations, the secondary α has adopted similar basal plane orientation as the adjacent primary α grains, although this is certainly not a “rule” of the phase transformation. With respect to texture, there was a weak $10\bar{1}0$ partial fiber aligned with the bar axis (Figure 4). EBSD scans made on longitudinal sections that contained the bar axis in the plane of polish revealed that there were elongated microtextured regions that had widths ranging from approximately 100 μm to 500 μm (Figure 5). Based on these data, specimens were cut transverse to the bar axis. As a consequence of the axial symmetry about the bar axis, there is an equal distribution of basal poles oriented between 0^o and 90^o to the loading direction. Therefore, the macroscopic texture of the as-received bar should not influence the grain orientation in which crack

initiation occurs as it could if there were limited grains in the gauge section or in highly textured plate, for instance.

B. Mechanical tests

The primary purpose of the present study was to create facets by various testing methods in order to study their characteristics. As a result, no extensive data acquisition was made during the tests, however, the lives of the fatigue specimens and the time to failure of the static loading experiments reveal some potentially important trends. For instance, the specimen that was continuously cycled at 95 pct. of the yield strength failed after 138,840 cycles while the specimen subjected to 2 min dwell periods at the same fraction of the yield stress failed after only 10,399 cycles, a debit of approximately 13x. To the authors knowledge, this is the first time dwell sensitivity has been reported in Ti-811. This alloy has previously not been investigated for dwell sensitivity because it is not an alloy used for jet engine rotors, however this finding is a potentially significant finding because there are Ti-811 fan blades in service.

With regards to static loading, the specimen loaded in 3.5 pct. NaCl failed after 10 hr 31 minutes at 758 MPa. The specimen statically loaded in air, in the absence of crack initiating notch and an aggressive environment, exhibited significantly longer life. This specimen was loaded for 426 hours at 758 MPa at which point the load was increased to the macroscopic yield strength, 798 MPa. Following the load increase, the specimen failed after 26 hours and 42 minutes.

C. Macroscopic fracture surface analysis

The fracture surfaces were all qualitatively similar in the sense that they contained facets and features, like dimples and shear lips, typically associated with overload failure. The regions between faceted growth and overload fracture were considerably different among the various specimens due to the different loading

histories, however, the features from this regime are not addressed in this manuscript due to the depth in which facets are addressed. While all specimens contained facets, the size and shape of the faceted regions were quite different. Secondary electron images of the cross sections of the as-fractured specimens are shown in Figure 6. The fracture surface of the cyclic specimen was typical of a fatigue failure, exhibiting surface crack initiation and a small, semi-elliptical faceted region near the surface of the specimen. The region of faceted growth transitioned to more conventional striation growth gradually, which is consistent with many observations of cyclic fatigue crack growth [22-27]. Striations were first observed in isolated grains at crack lengths less than 200 μm and became the dominant propagation mechanism at crack lengths > 1 mm. Striation growth proceeded with the macroscopic fracture plane remaining approximately perpendicular to the loading direction until the critical crack length was reached and overload fracture occurred resulting in the formation of a shear lip.

In contrast, the dwell fatigued specimen exhibited subsurface crack initiation and had a considerably larger faceted region that was on the order of 250 μm wide and extended approximately 3 mm from the circumference of the specimen into the gauge section. Similar elongated faceted regions were observed on all of the statically loaded specimens suggesting that the formation of such regions is unique to sustained loading. It is noteworthy that the length scale, aspect ratio and physical orientation of these elongated faceted regions is consistent with that of the microtextured regions observed in the as-received bar material (Figure 5). This correlation has possibly been overlooked in the past because the microtextured regions in the α + β forged pancake material analyzed by Sinha et al. [28] were approximately equiaxed in shape. In addition, Sinha et al. [28] did not explicitly identify where in the faceted region the crack started and thus a preferential growth could not be identified. Uta et al. [17] have studied the fracture surface specimen that failed during dwell fatigue loading that had elongated bands of microtexture similar to the material studied here. However, the authors used a 30 s dwell period and did not observe such a strong preference for the

faceted region to correlate with the underlying microtextured regions. This implies that cracks are growing faster through the faceted region during the sustained load than in the surrounding microstructure.

The specimen statically loaded in air was most similar to the dwell fatigue specimen in the sense that there was subsurface initiation and subsequent formation of an elongated faceted region and the fracture surface was relatively flat, aside from the shear lip. In contrast to the relatively flat fracture surfaces of the previous specimens, the macroscopic appearance of the specimen that failed by static loading in 3.5 pct. NaCl had substantial variations in height among the various locations on the fracture surface. This suggests, as later confirmed by more detailed fractography, that cracks grew inward from multiple locations at the surface of the sample until the remaining ligaments could no longer support the applied stress and failed by overload fracture. Several of the cracks entered via faceted growth while other cracks propagated by mechanisms which formed ductile fracture features until encountering a differently oriented microtextured region. It is notable that the crack propagation mechanism often changed from ductile to faceted with increasing crack length. This is in stark contrast to fatigue cracks which generally propagate by faceted growth at small crack lengths and striations or dimples at larger crack lengths. This observation suggests that the size of the crack tip plastic zone is not the dominant factor governing fracture topography during SCC as the cyclic crack tip plastic zone is during fatigue. Instead, the local fracture mode appears to be much more strongly dependent on local orientation.

D. Facet topography, spatial and crystallographic orientation analysis

The individual facets within the elongated faceted regions on all of the specimens appeared qualitatively similar under relatively low magnifications of 50x to 100x. The diameters of the thousands of individual facets that constituted the larger faceted regions described above were consistent with the diameters of the α grains as measured by EBSD and from the backscattered electron micrographs. In addition, some facets

were elongated with aspect ratios between 2:1 and 3:1 consistent with metallographic observations made on transverse sections of the as-received material. All of the fractured specimens were examined optically and with the SEM. The spatial and crystallographic orientations of several grains were also determined directly from the as-fractured surfaces.

1. Continuous cycling

There was a single clearly identifiable fatigue crack initiation site in the specimen loaded by continuous cycling. This region is shown at two levels of magnification in Figure 6 and Figure 7. Although there was no large, continuous faceted region consistent with the microtextured regions in this specimen there were many facets were observed at the crack initiation site (Figure 7). While some of the facets directly bordered one another, there were many locations separated by sharp, planar features such as those identified as numbers 2 and 3 in Figure 7. In the strictest sense, these could be called facets, but we reserve that term for the more planar features identified by the remaining numbers (1, 4, 5 and 6) that are formed by transgranular fracture through a primary α grain with a fracture plane nearer the basal plane than any other low index plane as will be shown later. Except for the initiation facet, there were markings on the facet surfaces that were indicative of the local crack propagation direction (Figure 8). Subsequent facet surfaces were observed to be progressively and continuously more rough with increasing crack length. In addition, the number of steps on the facet surfaces seemed to increase in density with each grain boundary encountered by the crack front. For the case of continuous cycling, this is related to the increase in the cyclic crack tip plastic zone size with increasing crack length [27] which results in a larger fracture process zone on each subsequent cycle. At high magnifications while utilizing the TLD, striations were occasionally visible on some facets. Two examples are shown in Figure 9 where, on the left, the striations resemble slip steps on the facet surface while, on the right, they resemble more conventional striations. At a crack length of approximately 100 μm, the spacing of these striations is on the order of 150 nm cycle^{-1}.

The spatial and crystallographic orientations of all the facets identified in Figure 7 (except for H2-1-7) were determined using the combined EBSD/quantitative tilt fractography technique. The results have been compiled in Figure 10 which shows the orientations of each fractured grain with respect to the loading direction and also with respect to the facet normal direction. A total of seven individual EBSD patterns were collected and indexed from the first grain to fracture (H2-1-1) while two patterns were collected from the remaining grains. Initiation occurred within a primary α grain that had its c-axis oriented 24^{o} from the loading direction. The facet normal angle was 27^{o} and the fracture plane was determined as being parallel to the basal plane for all seven indexed patterns within the resolution of the technique. The spatial and crystallographic orientations of this primary α grain initiation site are consistent with observations made on fatigue crack initiation facets in α grains in continuously cycled Ti-6Al-4V [29,30] and Ti-6246 [31,32] specimens with bi-modal microstructures. In addition, despite being near the surface of the specimen, the orientation of this grain is such that it could not have formed a slip band extrusion on the surface of the specimen as the only available <a> slip system which could intersect the specimen surface has nearly zero resolved shear stress.

Two of the grains (H2-1-2 and H2-1-3) directly adjacent to the crack initiating grain have their c-axes nearly perpendicular to the applied loading direction. In this orientation, the maximum resolved shear stress is on the prismatic <a> slip systems and there is nearly zero resolved shear stress on the basal plane. While there are also suitably oriented <c+a> slip systems, the higher critical resolved shear stress of these systems [33] imply that the grains would tend to deform by prismatic <a> slip. Because these two grains did not fracture on a flat, continuous faceted plane, the average fracture plane was determined over several areas spanning ~ 8 μm each on the fracture surface. After correcting for this average fracture plane

normal, the plane of fracture was determined to be near $\{10\bar{1}0\}$ for both grains. The average fracture plane normal for these regions was determined to be 41° (H2-1-2) and 25° (H2-1-3). The size, appearance and spatial orientation of these regions are consistent with the underlying microstructure being transformed β based on previous work conducted on bi-modal Ti-6Al-4V in which there was direct observation of the fracture surface and the underlying microstructure [30].

The remaining facets, H2-1-4 through H2-1-6, can be characterized as transgranular propagation facets through primary α grains. These facet normal directions made angles (in order) of 36°, 40° and 44°. The crystallographic plane of fracture was near the basal plane for all facets, however, there was a slight deviation from the basal plane observed for all specimens with facet H2-1-5 being the furthest, at an angle 5°. It is believed that these discrepancies can be attributed to errors introduced to the spatial orientation calculation by the increased facet surface roughness and the formation of steps as discussed in depth by Pilchak et al. [27]. Thus, all of these grains are in orientations that could have easily formed a slip band on the basal plane followed by cracking along that slip band.

The transformed β regions adjacent to the primary crack initiation facet were in elastically and plastically soft orientations. The crack initiating grain was in neither a hard nor a soft orientation as it was capable of slip on the basal plane. However, the spatial orientation of the facet also resulted in a considerable resolved normal stress on the facet plane, which has been suggested as being necessary for crack nucleation during continuous cycling fatigue of Ti-8Al-1Mo-1V [2]. Crack initiation occurs in the primary α grain because alloy partitioning which during thermomechanical processing of the alloy results in higher Al content in this constituent. Thus, it is more prone to planar slip [33] than the transformed β regions which also have many α/β interfaces that can form pileups under certain circumstances [34,35] which can

presumably result in delayed crack initiation [4]. However, definition of a detailed, mechanism-based understanding of the crack nucleation process for the continuously cycled specimen tested here is still unclear.

It is clear, however, that the initiation mechanism is not the result of a classical cleavage mechanism. The crack initiation facet is inclined to the loading direction and has formed on a plane in which slip has previously occurred. Furthermore, spectrum loading experiments [22,27] have shown conclusively that facets do not form during a single load cycle during continuous cycling but rather that the crack tip advances incrementally, cycle-by-cycle through each individual grain. Then, depending on the details of the local grain boundary structure, there may be an incubation period [36] before the crack begins to propagate into the next grain. The incubation period would be governed by microstructural factors such as crystallographic misorientation, grain boundary orientation and the degree of coplanarity between the current crack plane and the preferred crack propagation plane in the adjacent grain. Since this is a plasticity controlled growth mechanism, the local stress intensity range would be the dominant factor driving crack extension as opposed to exceeding a critical normal stress as in classical cleavage.

Subsequent faceted propagation occurred through nearby primary α grains that were also inclined to the loading direction. As shown in the inverse pole figures (Figure 10), a total of seven EBSD patterns were collected from the crack initiation facet (H2-1-1) along a horizontal line spanning the diameter of the facet. These points have been plotted on 0001 and $11\bar{2}0$ equal angle projections in Figure 11, which also shows a typical four of the seven total patterns acquired from this facet. Despite part of the detector being shadowed, these patterns are high quality and allow for accurate determination of the underlying grain orientation. In this representation, it is evident that collectively these patterns reveal a ~10^{o} lattice rotation

about [0001]. EBSD measurements made near slip bands and cracks on the polished surfaces of continuously cycled four-point-bend fatigue specimens [30] revealed no detectable lattice rotation in a plane transverse to the facet plane. Thus, the lattice rotations shown in Figure 11 are most likely related to the facet formation process although additional work is needed to understand their significance.

2. Static loading in air

It was more difficult to locate the crack initiation site in the specimen statically loaded in air compared to all of the others investigated in the present study. This was because the facet surface topography (roughness), which was the primary indicator of crack length in the continuously cycled specimen, was relatively consistent throughout the entire faceted region. Several representative propagation facets are shown in Figure 12. These facets had markings on their surfaces that corresponded well with the overall sense of crack propagation. The areal density of these markings on the facet surface and the orientation of the markings were observed to change abruptly at grain boundaries. After examining several millimeters of the faceted region at magnifications greater than 800x, a single facet was identified at a subsurface location that had the planar, featureless surface topography characteristic of crack initiation facets. This facet is identified by the number 1 in Figure 13. The surrounding facets can be characterized as propagation facets and were observed to be both inclined and nearly perpendicular to the loading direction. While the test was conducted in laboratory air, it is important to note that the facets formed at sub-surface crack initiation sites, were not surface connected and were therefore propagating in high vacuum.

Regardless of spatial orientation, the propagation facet surfaces all had a similar appearance which is shown in the lower portion of Figure 13. This surface topography is considerably different than that observed on the continuously cycled specimen and appears ductile. The markings on the facet surface had a distinct directionality which was consistent with the macroscopic crack propagation direction although the

orientation of these markings often changed substantially at grain boundaries suggesting that the crack propagation path was strongly dependent on crystallographic orientation, more so than those facets on the continuously cycled specimen. In general, the size and shape and density of these markings on the facet surfaces remained relatively constant throughout the entire faceted region. On each facet, there were typically several large ridges extending along the crack propagation direction. These ridges had several smaller ridges, or tributaries, branching off from it at an angle to the overall crack propagation direction. These tributaries became gradually smaller until they eventually were indistinguishable from the flat part of the facet surface between the ridges.

The top of the primary ridge was peak shaped and often came to a point suggesting that these features were formed by plastic flow of the α phase. Between the larger primary ridges, there was another set of shallower ridges that had similar shape. There were occasionally acicular features on the facets located near the ridges that were typically less than 100 nm long and 25 nm wide. In some locations, the features appeared as if they were particles sitting on the facet while in others they appeared to be partially embedded. They became most apparent on the facets only when imaged with the TLD. The particles appeared bright when imaged with secondary electrons and were indistinguishable from the rest of the facet when imaged with backscattered electrons, other than contrast changes due to surface roughness. Although these features are often associated with ridges, their significance in the formation of the ridge markings is not entirely clear as the frequency of ridges far exceeded the density of particles.

The crystallographic orientations of the initiation facet and five propagation facets (Figure 13) were studied in detail and the results have been plotted on the inverse pole figures in Figure 14. The initiation site, facet 1, had a normal that was 23^{o} from the loading direction while the propagation facets at the smallest crack length (facets 2 and 6) had angles of 18^{o} and 11^{o}, respectively. With regards to the plane of fracture, facet

1 is approximately 5° from the basal plane while facets 2 and 6 have fractured on planes approximately 15° from (0001). Similar to the case of continuous cycling, the crack initiated within a grain whose [0001] direction was inclined to the loading direction (~25°). Thus, the grain in which the crack started was oriented such that there was sufficient resolved shear stress for slip on the basal plane at the applied stress. The nearby propagation facets were less inclined, however, than those surrounding the continuous cycling initiation facet. It is also noted that the first propagation facets, 2 and 6, were also in an orientation where they could deform easily by basal slip, both having their c-axes more inclined to the loading direction than the crack initiating grain. However, despite the almost certain presence of basal slip bands, the crack clearly propagated along a crystallographic plane that was inclined to the basal plane and closer to $\{10\bar{1}7\}$.

Of the facets analyzed at a slightly longer crack length (facets 3, 4 and 5 in Figure 13), facet 3 was crystallographically oriented for easy basal slip like those grains near the initiation site, however it fractured ~15° from (0001) with a facet normal angle of 14°. Facet 3 also had two different underlying grain orientations as evidenced by the loading direction pole figure, however when we accounted for the difference in fracture plane normal amongst the various regions on the facet where EBSD patterns were collected, the crystallographic fracture plane was similar for all data points measured. The c-axes of facets 4 and 5 are oriented only 4° and 8°, respectively, from the loading direction. However, despite the high resolved normal stress on the basal plane of grain 4, it fractured on an irrational plane that was ~6° from the loading direction while grain 5 had highest normal stress on the irrational plane near $\{10\bar{1}7\}$, yet fractured precisely on the basal plane.

In this specimen, the initiation grain and the first few neighboring grains were in neither a hard nor soft orientation. In contrast to the continuously cycled specimen, the propagation facets were less inclined to the loading direction. Under sustained loading, this might be expected because, according to fracture mechanics [37,38], cracks propagating in mode I have the highest strain energy release rate per unit crack advance and thus would be expected to be preferred under sustained tension loading, assuming there is a crack extension mechanism available to support this. This may help explain why the crystallographic plane of fracture can be either (0001), or inclined to it. The fact that $\{10\bar{1}7\}$ occurs more frequently may be related to the fact that there are six $\{10\bar{1}7\}$ planes and only one basal plane, so it is more likely that a $\{10\bar{1}7\}$ plane will have higher resolved normal stress. The fact that the experimental data doesn't rigorously support this speculation (e.g. facet 4) is likely related to crack front incompatibility and local neighborhood effects resulting in grain level stress states considerably more complicated than when it is assumed each grain experiences a simple 'uniaxial' load [39].

This analysis has shown that there is not necessarily a unique facet plane during static loading in air, although the preferred fracture plane appears to be nearer to $\{10\bar{1}7\}$ than to (0001). While the formation of a slip band followed by separation of the slip band due to a normal stress can describe the formation of the initiation facet, it fails to describe the formation of the subsequent propagation facets because $\{10\bar{1}7\}$ is not a slip plane and it also has essentially zero resolved shear stress. Furthermore, although the formation of faceted features is typically associated with brittle fracture, the ridges on the surfaces of the propagation facets could not have been formed without localized plastic deformation. As will be shown subsequently, similar features were observed on the stress corrosion and dwell fatigue crack propagation facets. Therefore, discussion on the mechanism of facet formation is reserved until all data has been presented.

3. Static loading in 3.5 pct. NaCl

The specimen in the as-received condition that was statically loaded in 3.5 pct. NaCl exhibited surface crack initiation emanating from the scribe lines, however, none of these were directly connected to any of the faceted regions. Furthermore, there were no faceted initiations observed that appeared to be the result of surface slip band extrusions like those reported by Zhang and Vereecken [40]. There was one small region of facets (Figure 15) that was within a few microns from the surface of the specimen whose features indicated that the crack was running away from the surface of the specimen. This suggests that these facets were formed at a very small crack length after surface initiation in grains not suitably oriented for faceted crack propagation. Three of the facets from this region were analyzed in detail, labeled H3-1-1, H3-1-2 and H3-1-3 in Figure 15. All three facets were substantially inclined to the loading direction, having facet normal angles of 31^{o}, 32^{o} and 37^{o}, respectively. With respect to the loading direction, the c-axis of all three grains was inclined between 40^{o} and 47^{o} to the loading direction (Figure 16). Similar to the case of static loading in air, all of the facet planes near the initiation site were coincident with an irrational {hkil} plane that was inclined to the basal plane, between 6^{o} and 14^{o} in this case. Slip traces were evident on some facet surfaces (H3-1-2 in Figure 15, for example), however the slip traces were not parallel to the steps or ridges on the facet surfaces that were indicative of the local growth direction.

Additional propagation facets were analyzed in a different faceted region near the surface on the opposite side of the specimen where the crack was growing towards the free surface (Figure 17a). Similar to the specimen statically loaded in air, these propagation facets were typical of those observed throughout the rest of the faceted regions in this specimen. At longer crack lengths, the ridges on the facet surfaces were more similar in appearance to those in the specimen statically loaded in air except there were almost no tributaries extending from the primary ridges transverse to the primary growth direction as there were in the specimen statically loaded in air. The difference in the surface topography is most likely due to the

difference in environment at the crack tip. The facets in Figure 13 were formed before the crack was surface connected and therefore was propagating in a vacuum while the facets in Figure 17 were formed in the presence of a mildly corrosive 3.5 pct. NaCl solution. The main difference between the facets on the two specimens is the tributaries which branch out from the primary ridges on the statically loaded specimen (Figure 13), but not the 3.5 pct. NaCl solution (Figure 17). In addition, the peaks of all the ridges exposed to 3.5 pct. NaCl seemed to have been "smoothed" by the electrochemical reactions that occur at open circuit potential. On the other hand, the ridges on the facets of the specimen loaded in air (Figure 13) remain in the state in which they were formed. Examining the spatial and crystallographic orientations (Figure 16) of these propagation facets revealed that the facet normal directions were 7^{o} and 8.7^{o} from the loading direction. The [0001] axis of grain H3-1-4 was parallel to the loading direction, yet it fractured on a plane approximately 5^{o} from (0001). In contrast, [0001] of grain H3-1-5 was ~19^{o} from the loading direction with a fracture plane approximately 14^{o} from (0001), or 1^{o} from $\{10\bar{1}7\}$.

Between the primary ridges on the specimen tested in 3.5 pct. NaCl, there were smaller ridges approximately 100 nm to 200 nm long that also tended to align in the nominal direction of crack propagation as in Figure 17b and Figure 17d, for example. Images acquired with the TLD reveal that the ridges behave in a number of different ways compared to the steps on continuously cycled specimens [4,30]. These are illustrated by letters A through J in Figure 17b and Figure 17d which show facets H3-1-4 and H3-1-5. Some ridges are observed to get smaller until they become indistinguishable from the facet surface as indicated by letter B. The ridges are observed to interact in a number of ways at grain boundaries, which are identified by line segments A-A' and A-A'-A''. For instance, at location A', a new ridge is formed in the grain boundary whereas one ridge approaching the boundary at F gives rise to one larger ridge in the adjacent grain. However, at location G, a ridge is arrested at the grain boundary and not even a small ridge is

emitted into the adjacent grain. While these ridges were all perpendicular to the grain boundary, location H shows that the ridges also may change orientation at the grain boundary and propagate parallel to the boundary before becoming orthogonal to the boundary and advancing into the next grain. Two ridges that form at a grain boundary can coalesce once inside the grain as shown by letter C, however, the grain boundary is not necessary to develop a ridge as indicated at letter D. In general, all of the ridges exhibit some degree of undulation however, the primary ridges goes through extremely large curvature changes on some parts of the facet as indicated by letters E and J.

Although some ridges are observed to form internally on facets, it is clear that the crack propagates sequentially from grain to grain and there is no evidence for multiple internal initiations ahead of the primary crack tip which is characteristic of quasi-cleavage in quenched and tempered steels [41]. The formation of such features must involve considerably more localized plasticity than when the crack propagates along a preexisting basal slip band. This behavior is entirely different from the observations made in the continuously cycled specimen where the number of steps on the facet surface increased with each grain boundary encountered. Also, during continuous cycling, the overall facet surface roughness increased with increasing crack length due to the increase in the cyclic crack tip plastic zone size. In contrast, there was no direct correlation between facet surface topography (roughness) and crack length observed here despite the fact that the monotonic plastic zone size larger than the cyclic one [38].

4. Dwell fatigue

In addition to the primary and secondary initiation sites identified in the low magnification image of the fracture surface in Figure 6, another five subsurface secondary initiation sites were identified near the primary initiation site as shown in Figure 18. At least six other subsurface initiation sites were identified throughout the rest of the faceted region that extended towards the other side of the specimen, although

the search was by no means exhaustive. Due to the subsurface initiation, the crack would have been propagating in high vacuum throughout the faceted region in this specimen.

The primary initiation site (Figure 19) serves as a good example to demonstrate the necessary characteristics to be classified as an “initiation site”. The term “primary” implies that the location was where the first crack formed during testing for reasons that will become apparent below while the term “secondary” only implies that the initiation event occurred after the primary one. The fractographic analysis is not able to discern the order of subsequent initiation events. This terminology is consistent with that of Uta et al. [17] and also supports their observation of multiple initiation events within a single microtextured region during a dwell fatigue test of IMI 834. The facet topography in this region is consistent with that on the specimen statically loaded in air, with ridges extending along the direction of crack propagation. These markings lead back to the intersection two facets on the fracture surface, H2-2-1 and H2-2-2, which are shown at a higher magnification in Figure 20. There were steps on the surface of facet H2-2-1 and ridges on the surface of facet H2-2-2, both leading away from the grain boundary (segment A-A’). This implies that the crack initiated at the grain boundary where these two particular planes met. It is noted that there is extremely good mating between the facet planes over the length of the boundary which suggests that this is a primary α / primary α boundary as opposed to a primary α / retained β / primary α or a primary α / retained β / transformed β boundary. After the crack initiated at the boundary, it propagated by faceted growth through the surrounding grains labeled H2-2-3 through H2-1-7 and beyond.

Facet H2-2-1 was more planar than any of the adjacent facets and had the smooth surface topography consistent with the initiation facet on the continuously cycled specimen. This facet normal was 41.2^{o} from the loading direction while the adjacent facet normal, H2-2-2, was less than 3^{o} from the loading direction. These facet planes are near the maximum resolved shear stress and resolved normal stress orientation,

respectively. The subsequent propagation facets, H2-2-3 through H2-2-6, were also in near-maximum resolved normal stress orientations with facet normal angles of 8^o, 7^o, 8^o and 6^o, respectively. With regards to facet topography, facet H2-2-2 had a series of parallel, shallow ridges extending away from the grain boundary initiation site (Figure 19). With increasing crack length from the initiation site, these ridges became increasingly larger and began to exhibit branching as shown on facet H2-2-7. Crack front arrest marks, with spacing of 1.5 μm to 2.0 μm, were also evident on the facet surfaces at crack lengths greater than ~20 μm and became more apparent at magnifications of 500x to 1000x at crack lengths of ~100 μm (Figure 21). The primary ridges that are parallel to the local crack propagation direction are generally orthogonal to the crack front arrest marks. If not for these arrest marks, the dwell facets would be indistinguishable from those formed during static loading in air (but propagating in vacuum). It is noted that several arrest marks can be observed within a single facet indicating that these are neither cleavage nor quasi-cleavage facets as the observed characteristics do not conform to the definition of either term as they were originally used [27,41]. It is worth mentioning that Meyn [42] has observed crack front arrest markings on facet surfaces of Ti-811 subjected to static loading in hydrogen gas. Considering that similar markings were not observed on either of the statically loaded specimens, we are confident that the crack front arrest markings observed on dwell fatigue facets were formed during the unload/reload cycle. The markings were also observed to drastically change direction at some grain boundaries suggesting that this mechanism of faceted crack growth is highly crystallographic.

Surprisingly, neither the facet topography nor the crack front arrest mark spacing changed significantly with increasing crack length throughout the entire several millimeter long faceted region (Figure 21). At crack lengths greater than ~1 mm from the primary initiation site, the crack front arrest mark spacing was only on the order of 2.0 μm to 3.0 μm, just slightly larger than that measured at crack lengths between 20 μm and 100 μm. The facets consistently had ridges extending in the direction of local crack propagation and there

were often adjacent facets with varying areal densities of ridges. Presumably, this is an orientation dependency although no attempt was made here to quantify it. The effect of the unload/reload cycle on the primary ridges and facet topography is shown in Figure 21. The crack front arrest markings are similar to striations in the sense that they denote the occurrence of one unload/reload cycle, but because of their curved shape marking the crack front, they could not have formed by intersection of slip bands with the fracture surface and thus could not have formed by Laird's classical "sliding off" mechanism [43].

The crystallographic plane of fracture for the two grains involved in the crack initiation process and several of the subsequent propagation facets was investigated using the tilt fractography / EBSD technique and the results have been reported in Figure 22. With respect to the loading direction, the c-axis of grain H2-2-1 is inclined approximately 43^{o} while the remaining propagation facets all have c-axis inclinations between 8^{o} and 26^{o}. After accounting for the spatial orientation of each facet, the crystallographic plane of fracture was identified as being less than 1^{o} away from the basal plane for facet H2-1-1 and inclined between 16^{o} and 22^{o} to the basal plane for the remaining propagation facets. The crystallographic misorientation angle between grains H2-1-1 and H2-2-2 was 48.6^{o} indicating that this is a high angle boundary. Furthermore, the potential for slip transfer was investigated by the method described elsewhere [4] and it was found that there were no slip systems suitably aligned for transfer through the grain boundary. Thus, it is reasonable to conclude that this grain boundary was amenable to the formation of a dislocation pileup of significant strength.

The spatial and crystallographic orientation of facet H2-2-2 was measured a second time in a different SEM to confirm that the facet plane was indeed not coincident with the basal. In addition, during this second analysis, seven EBSD patterns were collected along a line extending perpendicular to the facet boundary towards grain H2-2-4. These orientations are shown on the inverse pole figures in the bottom of Figure 22

which clearly reveals that the fracture plane is inclined 15° to the basal plane, making it near to $\{10\bar{1}7\}$. Six of the seven patterns from the analysis are shown to provide an indication of pattern quality and the corresponding indexed orientations from all seven patterns are shown on pole figures in Figure 23. The orientations also exhibit a rotation of 10° about [0001] over a distance of approximately one grain diameter.

The facets on all of the grains surrounding the initiation site, except H2-2-5, were oriented such that the c-axes were inclined 20° to 25° to the loading direction indicating that they were capable of basal slip. However, all of the facet normal directions were nearly parallel to the loading direction, with the largest deviation being ~7°, indicating that the fracture plane was not the basal plane, but rather inclined to it as shown in Figure 22. Other facets surrounding the primary initiation site, from which EBSD data was not collected, exhibited deviations as large as 16°. Although these grains should have been capable of basal slip, and likely developed basal slip bands during loading, they did not fracture on this plane. Instead, the fracture planes deviated between 12° and 23° from (0001) which is similar to the specimens fractured by sustained loading in air and in 3.5 pct. NaCl. The similarity in spatial and crystallographic orientation and facet surface topography among the facets formed by these three types of loading suggests that all of the cracks are propagating by similar mechanisms. The differences in crack growth rates and facet appearance are most likely related to the crack tip environment.

The secondary initiation site identified on the dwell specimen in Figure 6 was also examined with tilt fractography and EBSD and the results are shown in Figure 24. The initiation facet (B1) was identified by its smooth, planar surface topography, which became more apparent at large stage tilts. This facet had a normal that was 25° from the loading direction while the two neighboring propagation facets, B2 and B3, made angles of 14° and 20°, respectively. After accounting for the spatial orientation, the fracture planes

were determined to be between 2° and 5° from (0001) for grain B1, ~15° for grain B2 and ~16° for B3. These observations provide additional confirmation for the initiation mechanism observed at the primary initiation site. It is argued that the primary site was more favorable for early crack initiation due to the better matching of the fracture planes in the grain boundary along with the higher resolved shear stress for slip on the basal plane of grain H2-2-1.

IV. Further discussion: Dwell fatigue crack initiation and propagation

The fractographic and crystallographic observations presented above provide further support for the reports of Sinha et al. [7,8] and Uta et al. [17] regarding the crystallography of dwell fatigue crack propagation facets. Both authors have reported that dwell fatigue crack propagation facets were inclined between 10° and 20° to the basal plane in the near-α alloys Ti-6242 and IMI834, respectively. Using the same technique to locate initiation sites as we have reported here, namely, tracing the fine markings on the facet surfaces to a convergence point, Uta et al. [17] were able identify a primary initiation site and several secondary initiation sites. The authors characterized each initiation site as containing a "pure cleavage facet with no local marks" that was surrounded by "quasi-cleavage" propagation facets. Ignoring the inconsistencies regarding the use of the words "cleavage" and "quasi-cleavage" to describe both types of facets [27], it is noted that crystallographically, the primary initiation site observed by Uta et al. [17] is consistent with our observations. Specifically, there is one grain with it's c-axis inclined to the loading direction such that it can deform by basal slip that faceted near the basal plane resulting in a microscopically smooth, planar fracture surface. Adjacent to this is another grain whose c-axis less inclined to the loading direction that forms a facet on an irrational plane inclined between 10° and 20° to the basal plane and that has markings indicative of crack propagation. Unfortunately, Uta et al. [17] reported neither the spatial orientation of the facet normal directions nor the facet normal inverse pole figures so no further comparison to their results

can be made here. The spatial and crystallographic characteristics of the propagation facets analyzed here are, however, consistent with the measurements made on dwell facets by Sinha et al. [7,8].

The direct observation of several dwell fatigue crack initiation sites (both primary and secondary initiation in the present study and by Uta et al. [17] in a different alloy) that contain pairs of adjacent primary α grains similar to those described above is potentially significant as it seems to both confirm and contradict a number of things considered to be characteristic of dwell fatigue failures. First, these results confirm that there is indeed a pair of grains involved in the crack initiation process as first proposed by Evans and Bache [6]. Here, despite the relatively high volume fraction of transformed β, both of the grains involved in the initiation event were primary α grains. The adaptation of the Stroh model initially proposed by Evans and Bache [6] contends that slip in the soft grain and the formation of a dislocation pileup is necessary to induce slip on the basal plane of the hard grain. This is necessary to obtain the necessary critical combination of shear stress (or strain) and tensile stress normal to the slip plane that is required for facet formation. This requirement for facet formation has percolated throughout the dwell fatigue literature, however, the original citation for this requirement is due to the work of Wojcik et al. [2], who studied the facets formed on large single colonies of Ti-811 subjected to continuous cycling. All but one of the single colonies studied by Wojcik et al. [2] had the basal plane oriented such that there was sufficient resolved shear stress for slip. Consequently, it would be expected that this would be the plane which accumulates damage fastest leading to crack initiation and propagation *during cyclic loading*. The applicability of the results of Wojcik et al. [2] to dwell fatigue crack initiation in a polycrystalline material is not immediately obvious. The tilt fractography / EBSD analysis presented above showed that the first propagation facet was actually parallel to an irrational plane near $\{10\bar{1}7\}$ that is incapable of slip. In addition, the difference in surface topography between the facets formed during continuous cycling and dwell fatigue loading are

unmistakable. There is no reason in which the mechanism that forms a smooth facet directly on a basal plane that is inclined to the loading direction and the mechanism that forms a facet with ridges and rough topography that is perpendicular to the loading direction and parallel to an irrational {hkil} plane inclined 10^{o} - 15^{o} to the basal plane should be the same. Thus, the requirement for slip on the basal plane of the hard grain prior to fracture is unfounded and does not appear to be necessary based on our observations.

The second point that the experimental results presented here draw into question does not relate to the Stroh model itself, but rather how a specific orientation has been attached to the phrase “soft grain”. With the use of EBSD analysis [44,45] and careful serial sectioning [28], it was observed that dwell fatigue cracks generally initiated in regions of the microstructure which had both hard and soft microtextured regions. The soft regions were those which were in an elastically and plastically more compliant orientation meaning that their c-axes were nearly perpendicular to the loading direction and they could deform by prismatic <a> slip. Based on these experimental studies, the understanding of the “source slip band” in the originally proposed Stroh-like model (Figure 1) evolved into meaning a soft grain oriented for prismatic <a> slip. A number of authors [46-49] have addressed the phenomenon of room temperature creep in the “soft grain” and the resulting stress redistribution onto the “hard grain” using finite element based crystal plasticity simulations. While there are differences among the results of the models, they generally agree on the fact that stress redistribution within the microstructure results in the formation of large stresses at, or near, the interfaces between hard and soft microtextured regions, and the spatial orientation of the interface can either increase or decrease these stresses. This latter point is useful understanding why a crack forms at one location within the component as opposed to others with nominally the same crystallographic misorientation. However, while the experimental observations [28] suggest this phenomenon is occurring on a length scale consistent with the microtextured regions, some models have attempted to employ it on the grain level [48,50]. In addition, the tilt fractography / EBSD analysis presented above suggests that the

"softer" of the two grains is one that can deform easily by basal <a> slip as opposed to prismatic <a> slip. The "harder" grain has it's c-axis inclined ~20^{o} to the loading direction implying that it is not truly a hard grain in the sense that <c + a> pyramidal slip is not necessarily enforced.

Finally, it is often reported [6,12] that when the applied load is below the macroscopic yield strength of the material, that facets are formed nearly perpendicular to the loading direction regardless of whether a cyclic or dwell waveform is imposed. The results from the facet normal calculations as a function of loading type have been summarized in Figure 25. In this plot, the initiation facets are represented by filled symbols. It is noteworthy that initiation facets were observed on all samples with an angle around 25^{o} (secondary initiation site in dwell specimen). The specimen that was statically loaded in 3.5 pct. NaCl exhibited facet angles both inclined and perpendicular to the loading direction. This is most likely related to the fact that the underlying grain orientation influences fracture topography as much or more so than crack tip plasticity does. This point is evidenced by the fact that fracture topography was observed to change from ductile to faceted growth with *increasing* crack length. Furthermore, all of these facets were formed below the macroscopic yield strength of the material, including those on the continuously cycled specimen, and thus the concept that facets should be normal to the loading direction appears to not apply here.

A. Phenomenological model for dwell fatigue crack initiation

Although the orientations of the grains at the primary initiation site of the dwell fatigue specimen have been identified, it is still necessary to describe how slip in the soft grain leads to crack nucleation in the boundary and subsequent faceted propagation through the harder grains. Due to the large inclination of the initiation facets, and the presence of ridges indicative of the occurrence of plasticity on the propagation facets, neither the crack initiation nor faceted growth mechanisms appear to be controlled by a simple normal stress criterion, e.g. by "cleavage," as some models have advocated [50]. In this section, a

phenomenological model for crack initiation and faceted propagation consistent with the experimental observations is presented. It is important to note that the dwell fatigue literature has been carefully considered while developing this mechanism, however, it may not be relevant for all alloy compositions and microstructural conditions. Recently, Brandes et al. [9,51] have shown dwell sensitivity in a single phase, equiaxed, polycrystalline Ti-6Al alloy that was thermomechanically processed via extrusion to have essentially no hard oriented grains. Even in this simple material system, a significant dwell debit was observed implying that this phenomenon is inherent in near-α (and perhaps other) titanium alloys. Whether or not a particular system exhibits a dwell debit in its service life would likely depend on a number of factors known to exacerbate the dwell effect, including but not limited to: alloy composition, microstructural condition, interstitial content (O, H) and, perhaps most importantly, the presence of hard microtextured regions which provide an easy, continuous path for faceted growth.

The primary initiation site of the dwell fatigue specimen was studied extensively and even re-visited on several different occasions. The spatial and fracture plane orientations presented above were verified in two different electron microscopes to ensure consistency. It is emphasized that the fracture planes were determined from a location on the facets that did not contain any steps and therefore the explanation offered by Pilchak et al. [27] for deviations from the basal plane due to facet roughness does not apply here. Therefore, these results are believed to be an accurate representation of the true orientations and fracture planes of the first grains to fracture during a dwell fatigue test. The discussion of the crack initiation process will be limited to only these two grains, however, the reader is reminded that these grains are believed to exist within some volume of stressed material near the interface of a hard and soft microtextured region which would be consistent with previous experimental observations [8,17,44].

Consider the pair of grains in Figure 1 and assume the hard grain is one that is oriented with its c-axis approximately 20^{o} from the loading direction while the neighboring soft grain is oriented for easy basal slip. Upon the application of a load, the soft grain deforms by basal slip. Since there are no closely aligned slip systems in the hard and soft grains, the grain boundary serves as a barrier to dislocation motion and a dislocation pileup is formed. During subsequent cycles, strain is accumulated in the basal slip band intensifying the stress concentration at the head of the pileup. The stress concentration induces normal and shear stresses onto the planes in the adjacent hard grain. However, Koehler [52] has pointed out that a substantial hydrostatic tension field is also created around the pileup that extends over an appreciable volume of material around the pileup. In titanium alloys, it has also been demonstrated that interstitial hydrogen is readily mobile at room temperature and that it will diffuse to regions of high hydrostatic tension, such as a crack tip [53]. Due to its low solubility in the hexagonal α phase, locally elevated concentrations of H can lead to the precipitation of a titanium hydride, which is a compound, often non-stoichimetric, based around TiH_x where x is between 1.5 and 2. The lattice parameter and crystal structure of the hydride depends on the stoichiometry of the hydride being face centered cubic when x is between 1.5 and 1.8 and face centered tetragonal when it is above approximately 1.8 [54]. As mentioned by Williams [55], the formation of TiH_2 is accompanied by an ~ 18 pct. change in volume which significantly strains the surrounding matrix. In strain-free metals, the transformation strain is so large that hydride formation requires the creation of prismatic <a> dislocation loops. However, Boyd [56] has shown that slip bands can serve as effective nucleation sites for hydrides by acting as interface dislocations and reducing the elastic misfit.

With regards to dwell fatigue, there are several possible ways in which hydrogen can influence the crack initiation process. The first possibility is that the hydrostatic stress field around the head of the dislocation pileup in the soft grain attracts hydrogen which leads to hydride precipitation. Following precipitation, a

crack could form either by fracture of the hydride followed by subsequent growth into the surrounding matrix, or localized plastic deformation at the particle / matrix interface could lead to void formation and subsequent crack extension. Another possibility is that which was suggested by Troiano [57] where hydrogen diffuses to regions of high triaxial stress and lattice defects which promotes microcrack nucleation upon reaching a critical concentration level. Hack and Leverant [5] have attempted to use this mechanism to explain dwell fatigue crack initiation in fully lamellar near-α alloys, but suggested that propagation occurs by the repeated formation and cracking of hydrides at the crack tip. There was no convincing evidence provided for either mechanism. The third, and most attractive based on the present experimental results, is that of "hydrogen enhanced localized plasticity" (HELP) [53]. As summarized by Robertston and Birnbaum [58], over a period of approximately 20 years, there have been repeated direct observations in the TEM that hydrogen influences the mobility of edge, screw, partial and grain boundary dislocations in ordered and disordered face-centered-cubic, body-centered-cubic and hexagonal-close-packed materials. This accelerated dislocation behavior under constant applied stress was observed in all metallic systems in which hydride precipitation would be expected and is observed. Of particular interest is their work on near-α titanium alloys in which Shih et al. [53] showed this behavior caused a localized softening effect in the α phase of Ti-4Al. Under positive pressure of H_2 gas, hydride precipitation, growth and subsequent fracture by cleavage of the hydride was observed. However, when observing dynamically growing cracks that were propagating too fast for hydride precipitation, a change in fracture mechanism from brittle hydride cleavage to localized ductile fracture was observed. In this mechanism, the dislocation enhancing H atmosphere resulted in slip localization, highly constrained plasticity and extremely localized fracture at regions of highest H concentration. On a fracture surface, this type of failure is manifested as tear ridges and dimples [58], both of which were observed on the facets in the dwell and static loaded specimens.

The HELP mechanism is clearly the most consistent with the experimental observations made on the propagation facets present study as it can help explain the localized formation of tear ridges on the facet surfaces. The occurrence of localized softening and slip resulting due to the hydrogen atmospheres is believed to accommodate the plastic strain required to locally form an instability on the facet surface, similar to a "neck" in a tensile test, leaving a ridge as the crack advances during the hold period. Further support for the role of hydrogen in dwell fatigue crack propagation can be found in the results of the spatial and crystallographic orientation analysis. Crack propagation from the first grain occurred on planes nominally perpendicular to the loading direction that were coincident with irrational {hkil} planes inclined between 10^{o} and 15^{o} to the basal plane as opposed to on (0001) as was observed during continuous cycling.

Reviewing the spatial and crystallographic orientations of the grains at the dwell fatigue crack initiation site (Figure 22) reveals that the harder grain, the first propagation facet, has a $\{10\bar{1}7\}$ plane oriented within ~2^{o} of the applied loading direction (maximum mode I component). Similar occurrences can be found in the surrounding dwell propagation facets as well as in the specimens statically loaded in air and in 3.5 pct. NaCl which, along with their similar surface topography, suggests that these facets all formed by a similar mechanism. We have already discussed why a facet in this spatial orientation would be preferred from a continuum mechanics perspective due to its high energy release rate, however, it has yet to be explained mechanistically why fracture occurs preferentially on irrational {hkil} plane as opposed to low index planes. This is a particularly intriguing problem considering that may of the basal planes are sufficiently inclined to the loading direction that it can be argued that they have dislocations present that, presumably, lower the cohesive strength of that plane from a defect-free crystal.

A number of hydride habit planes have been reported in titanium alloys depending on alloy composition [55] and hydrogen content [59], among other factors, including (0001), $\{10\bar{1}0\}$, $\{10\bar{1}2\}$, $\{10\bar{1}4\}$, $\{10\bar{1}7\}$ and $\{11\bar{2}3\}$. Of particular interest are the basal planes and those habit planes that are only slightly inclined to it, like $\{10\bar{1}7\}$ and $\{10\bar{1}4\}$ which are approximately 15° and 24° from (0001), respectively. These habit planes are inclined approximately the same amount from (0001) as the majority of the fracture planes observed on the dwell and statically loaded specimens. However, the habit planes mentioned above were primarily determined in binary experimental alloys created by float zone electron beam method, charged with H in a Sieverts apparatus and then heat treated and slowly cooled to produce large hydrides observable by optical microscopy. The presence of applied or residual stresses, however, can significantly affect the precipitation process [55,59-61] resulting in a change in the orientation of the preferred habit plane. In fact, the effect of elastic stresses on hydride precipitation and the habit plane orientation has been recognized since the early 1960's [62,63]. Under tensile load, the preferred habit plane is the one that is closest to perpendicular to the loading direction because it accommodates a portion of the large strain necessary for hydride nucleation. Perhaps only by coincidence, this is also the approximate orientation of the faceted fracture planes. It is worth mentioning that similar phenomenon have been observed experimentally [64] and addressed theoretically [61,65] for zirconium hydrides. In fact, it is generally accepted that stress-dependent hydride precipitation followed by subsequent fracture of the hydrides is the primary cause of early fracture of zirconium alloys used as structural components in nuclear reactors [64].

The coincidence of the crystallographic fracture plane with a hydride habit plane known to form under the influence of an externally applied stress provides circumstantial evidence that hydride precipitation is involved, however there is currently no direct evidence of this available on the fracture surfaces. Thus, it is useful to understand the facet surface topography associated with formation and/or fracture of a hydride

particle. Consider the fractographs from the study by Yeh and Huang [66] that have been reproduced in Figure 26(a) and (b). These facets were formed in Ti-6Al-4V by static loading a CT style specimen in H_2 gas of varying pressure at a variety of temperatures. The similarity between these facet surfaces and those on the Ti-811 specimens studied presently are unmistakable. The facets contain ridges of varying height extending in the direction of crack propagation with smaller tributaries branching off from them. There are disc shaped features on the surface of the facet formed in 505 kPa H_2 gas at 95 ^{o}C, but not on the facet formed in 101 kPa H_2 gas at room temperature. On the former facet, one of the larger disc-shaped precipitates appears fractured and there is evidence of void growth around the particle as it is sitting in a shallow dimple. These features were not observed on the latter facet (101 kPa; 20 ^{o}C) which instead had fine acicular particles sitting on the facet surface that were often associated with the ridges. Rusli [67] has described similar features on the facet surfaces of a Ti-8Al-1Mo-2V alloy fractured in ~10 kPa H_2 gas at a constant displacement rate of 0.5 mm min^{-1} after fatigue precracking. Rusli [67] has captured some of the particles in an acetate replica of the fracture surface and observed them directly in the TEM (Figure 26c). Based on selected area electron diffraction analysis, he reported that these particles were indeed hydrides that precipitated in the α phase. None of the smaller particles were observed to be fractured like the larger, disc-shaped particles observed by Yeh and Huang [66].

The finer, acicular shaped particles observed on the facets in Yeh and Huang's study [66] and also by Rusli [67] were similar in size and morphology to features observed on the propagation facets of the dwell fatigue and statically loaded specimens. An example from the former is shown in Figure 27, however it is noted that neither the chemistry nor crystal structure of this feature is unknown. Attempts to capture these particles in acetate replicas were made in the present study, however, none were found when observed in the TEM, suggesting that they were rigidly adherent to the facet surface, or that they were simply fractured titanium that appeared brighter in the TLD and were not actually a different constituent. Robertson and

Birnbaum [58] have argued that no single hydrogen-related mechanism can explain all experimental observations and it is likely that more than one operates in a given specimen. Thus, it is enticing to conclude that the HELP mechanism appears to dominate facet formation, although those hydride variants with habit planes perpendicular to the stress axis could precipitate and assist in the fracture process by promoting formation nearly parallel to their habit plane (and perpendicular to the loading direction). Since there is no evidence of fractured hydrides on any of the facet surfaces on the specimens studied here, it is likely that hydrides (if present) exert their influence through localized deformation at the particle/matrix interface. This type of deformation behavior can rationalize both ridge formation as well as the coincidence between the fracture plane and hydride habit plane. Because there was no hydrogen gas at the crack tip of any of the specimens in the present study, it is necessary to invoke the internal hydrogen content of the alloy as the source of hydrogen to account for the observed features in the dwell fatigue and creep specimens. Clearly, hydrogen was abundantly available in the SCC experiment, which is the exception. As mentioned previously, the frequency of the potential hydride particles on the facets was considerably lower than that of the ridges and so it is believed that the formation of these is not essential for ridge formation. It is possible, however, upon fracture the dilatational stress field is relaxed liberating hydrogen that can diffuse back to the crack tip and repeat the process. This last point is difficult, if not impossible to prove for bulk specimens, and to our knowledge there have been no observations of this in thin foil studies either, but the minimal constraint in thin foils could preclude this effect anyway.

Further support that hydrogen may play a role in dwell fatigue crack propagation process is contained within the crack growth rates as inferred from the features on the facet surfaces. The spacing of the crack front arrest markings was determined by projecting vectors into the plane of fracture using the quantitative tilt fractography method. The magnitude of the vectors could be related to a physical dimension through the known working distance, SEM magnification and image resolution. This ensures that the spacing

measurements are not subjected to uncertainties associated with those made on two dimensional images in which the feature of interest is inclined to the viewing direction. Near the initiation site and within the first several hundred microns, the arrest mark spacing was on the order of 1 μm to 1.5 μm per cycle while at longer crack lengths > 1.5 mm and throughout the entire faceted region, the crack front arrest marks saturated to a value between 2.0 μm and 3.0 μm per cycle. As a comparison, recall that the crack was advancing at a rate of approximately 150 nm cycle^{-1} (Figure 9) at a crack length of ~100 μm in the continuously cycled specimen. From this value, the crack front indicators on the continuously cycled specimen gradually increased with increasing crack length eventually evolving into classical fatigue striations. If internal lattice resistance were the only force responsible for retarding crack growth during dwell fatigue, the crack growth rate should increase monotonically with increasing crack length due to the cyclic crack tip plastic zone having a quadratic dependence on ΔK similar to the continuously cycled specimen. This is a potentially important observation, especially when considered in the context of two other relevant facts. First, the size and shape of the faceted region reflects the underlying microtextured bands that were observed in the as-received material and second, the apparent facet surface roughness of the dwell propagation facets does not increase significantly with increasing crack length. Both of these observations suggest that the fracture process is not controlled by localized plasticity, but rather is a time dependent growth mechanism. The fact that the size and shape of the faceted regions is similar to those of the microtextured regions in all of the specimens subjected to a sustained mode I loading condition implies that the crack grew preferentially through this region before extending into the surrounding microstructure. This assertion is further supported by results from non-destructive evaluation measurements performed on an additional sample from this study which did not fail after 26k dwell cycles. A sub-surface crack was identified in the gauge section of the specimen after reconstructing the entire volume with x-ray computed tomography (Figure 28). This data, shown from two orthogonal directions, reveals an internal flaw that is approximately 2.4 mm long, 0.25 mm wide and is oriented perpendicular to the loading direction. The size

and shape of this flaw is consistent with the size and shape of the microtextured regions observed in the as-received material as well as with the faceted regions observed on other specimens. This observation has important implications on variability of dwell fatigue life in laboratory specimens. For instance, the faceted region on the specimen studied in detail here intersected the surface of the specimen resulting in a larger stress concentration and exposure of the laboratory environment to the crack tip, both of which can accelerate crack growth rates through the non-faceted regions. In contrast, the specimen shown in Figure 28 had already experienced more than double the number of cycles and revealed no significant crack growth into the adjacent microstructure.

Under continuous cycling, crack growth rates are slower when the nominal fracture plane is parallel to the basal plane and is also perpendicular to the loading direction, i.e. there is no shear stress on the basal plane. This has been demonstrated for strongly textured Ti-6Al-4V by Bowen [68] as well as for single colonies of Ti-811 by Wojcik et al. [2]. Presumably, this is due to the higher critical resolved shear stress required for <c + a> dislocations to glide which would be required to permit crack tip opening to occur plastically as in Laird's classical mechanism for fatigue striation formation [43]. However, orientation dependencies and texture effects during dwell fatigue crack growth (and other waveforms which involve a sustained load) are arguably less well understood. As mentioned by Brandes [9], there are contradicting reports in the literature on the effect of dwell periods on fatigue crack propagation rates [15,26,69-74]. Some researchers find increased crack growth rates while others measure no difference and some even find reduced growth rates. The relevance of these studies has been called into question [9], however, since they generally focused on long cracks growing in air as opposed to internally initiated cracks that are not surface connected which are growing in a vacuum. The markings on the dwell and continuously cycled specimens that indicate the position of the crack front on successive cycles have shown that crack growth rates are invariably faster in the faceted region for the dwell fatigue specimen compared to the continuously

cycled one. In addition, having established that the size and shape of the faceted region is dictated by the underlying microtextured regions and that the crack forms within and propagates preferentially through these regions, it becomes clear that crack growth rates outside of the faceted region during dwell fatigue are even less important to the total life. The fact that crack growth rates measured on CT specimens are often insensitive and occasionally slower during dwell loading further suggests that the crack initiation and small crack growth stage are more critical to explaining the observed life debit. The reduction in the number of cycles to crack initiation due to dwell loading is obvious, however the considerably higher growth rates measured directly from the facet surfaces in the present study suggest that the faceted crack growth stage is equally, or even more important. This concept is consistent with the recent work of Toubal et al. [75] who have suggested that specimens which better resist crack propagation exhibit longer dwell fatigue lives, although the authors have not identified the particular importance of resistance to faceted growth.

Now that the preferred orientation of crack initiating grains and crack propagation grains has been identified, it is possible to discuss the effect of microtexture region size on dwell fatigue life. Consider the EBSD map of the transverse cross section of the dwell fatigue specimen collected approximately 1.3 mm below the fracture surface, but still well within the reduced section of the specimen, shown in Figure 29. These data illustrate that there is a range of sizes and aspect ratios of microtextured regions with c-axes near, or slightly inclined to, the loading direction (red hues) and so it becomes useful to understand why crack initiation might be favorable in one location compared to another. In addition, once a crack has initiated, it is useful to know which neighborhoods will facilitate faceted crack growth and ultimately lead to fracture of the component in comparison to those that result in crack arrest. For discussion purposes, consider the following simple example.

Two cracks initiate on the same dwell cycle at locations A and B in Figure 29a. They initiate at grains like those described in detail above that happen to be near the interface between “hard” and “soft” microtextured regions because of the locally higher stresses developed here due to load shedding [46]. After crack initiation, continued growth of the crack depends on its surrounding microstructure. based on the tilt fractography / EBSD studies, we have identified that grains with $\{10\bar{1}7\}$ planes nearly perpendicular to the loading direction provide easy propagation paths. Thus, in Figure 29b, we have color coded grains with high resolved shear stress on the basal plane, initiation grains, in blue, whereas the easy propagation paths are identified by the color red. Both cracks advance on each subsequent dwell cycle through their respective microtextured regions. Upon reaching the edge of the microtextured region, crack B is arrested because the soft oriented grains on the other side are able to accommodate its plastic zone, similar to what has been observed during continuous cycling [30,76]. The crack does not grow readily because there are no more basal planes suitably oriented for faceted growth. Crack A, on the other hand continues to propagate through the larger microtextured region until it too reaches a soft oriented grain. Outside of the faceted region, dwell fatigue cracks have been observed to propagate by more conventional striation growth [26] which is controlled by crack tip plasticity. Therefore, it is reasonable that the driving force for further crack propagation is proportional to ΔK, which would be considerably larger for crack A suggesting that it would most likely propagate to catastrophic failure. Thus, the size and shape of the microtextured region is the most important attribute affecting dwell fatigue life because, in materials with large microtextured regions, a concomitantly large internal crack can develop while the crack is still growing at high rates under relatively microstructure insensitive conditions until faceted growth is exhausted. Then, this internal flaw serves as the initial condition for the second stage of crack growth which appears to occur by more conventional striation growth mechanisms. For modeling purposes, it is likely that the size and

morphology of the microtextured region could be used to select an appropriate K solution to model subsequent plasticity controlled long crack growth.

V. Summary

Previously proposed dwell mechanisms based on hydrogen have been criticized in the past because of their inability to explain the relatively large strain accumulation associated with dwell fatigue. Measurements of bulk strain accumulation, however, include contributions from all of the grains within the sample that, because of recent experimental and modeling efforts, are known to be plastically deforming at room temperature. Thus, it would certainly be possible to have substantial strain accumulation at the component level while simultaneously forming and propagating a large internal crack by a process involving extremely localized plasticity, such as that afforded by the HELP mechanism.

Based on the experimental results presented here, and after careful, collective consideration of the relevant literature, we propose that the question regarding the role of hydrogen during dwell fatigue be revisited. Due to the large number of factors that influence dwell fatigue susceptibility and their apparently synergistic interactions, future experiments need to be carefully designed to probe a specific effect while maintaining the other factors constant. Experiments conducted in our laboratory [77] have shown an increase in dwell fatigue life with increasing hydrogen content. However, reexamination of the fracture surfaces in light of the present results revealed that the size of the faceted region varied from sample to sample. It was observed that dwell fatigue life increased with decreasing faceted region size. Perhaps only by chance, the relative size of these regions scaled inversely with hydrogen content. Since the hydrogen charging temperatures are too low to induce any change in microstructure and certainly too low to change texture, this implies that the effect of microtexture region size overshadows the effect of hydrogen, at least for bulk concentrations up to 230 ppm, which exceeds specification limits. This demonstrates the need to study simple material

systems in which one variable can be changed at a time to gain a more thorough understanding of all the individual mechanisms associated with dwell fatigue crack initiation and propagation. By understanding the individual contribution of each variable (such as microtexture region size, hydrogen content, texture, primary α volume fraction, environment) it would be possible to begin to understand the interrelations among them.

VI. Conclusions

Based on the analyses presented above, the following conclusions were reached regarding crack initiation and faceted crack growth that occurs under different loading conditions.

A. Continuous cycling

- Fatigue crack initiation occurred at the surface of the specimen in a grain whose basal pole was inclined 25^{o} to the loading direction.
- Subsequent propagation also occurred on basal planes that were inclined between ~22^{o} and 41^{o} to the loading direction, although some facets with unique surface topography were found to be {10-10} fracture planes.
- Markings on the facet surfaces that resemble fatigue striations indicated that the crack growth rate was on the order of 150 nm $cycle^{-1}$ at crack lengths as small as 100 μm.
- Facet surface roughness and crack growth rate increased with increasing crack length consistent with plasticity controlled crack propagation.

B. Static loading in air

- Subsurface crack initiation occurred on a facet inclined ~23^{o} to the loading direction producing a smooth facet nearly parallel to the basal plane.
- Subsequent crack propagation occurred on irrational {hkil} planes inclined between 7^{o} and 20^{o} to (0001). Around the initiation grain, the propagation facets were more inclined to the loading direction than at longer crack lengths. Several of the crystallographic fracture planes were consistent with known hydride habit planes, although no direct evidence of hydrides were found.
- The facet surface topography was consistent with that formed by cracking in small positive pressures of hydrogen gas consisting of tear ridges extending in the direction of crack propagation.

C. Static loading in 3.5 pct. NaCl

- Although no surface initiation facets were identified, it was evident that the preferred crack propagation plane was perpendicular to the loading direction regardless of the precise {hkil} plane.
- All of the facet planes analyzed were inclined between 5^{o} and 15^{o} to the basal plane in their respective grains.
- The facet surface topography consisted of ridges extending in the direction of crack propagation, similar to that observed on the specimen statically loaded in air, except that the environment may have altered some of the fine details on the ridges.

D. Dwell fatigue

- Cracks initiated at the intersection of a basal slip band in a grain oriented with a $\{10\bar{1}7\}$ plane nearly perpendicular to the loading direction. The basal slip band was inclined to the loading direction in a high resolved shear stress orientation (basal pole 42^{o} from loading direction) while the

preferred propagation planes were those in which maximum normal stress was resolved onto the $\{10\bar{1}7\}$ plane. Other irrational {hkil} planes near $\{10\bar{1}7\}$ were also observed less frequently.

- The microscopic surface topography of these facets were consistent with those formed by static loading in air and 3.5 pct. NaCl suggesting that they have all formed by similar mechanisms and that the environment and unload/reload cycles act to modify the rate of crack propagation. Based on the time to failure of each specimen, loading in 3.5 pct. NaCl appeared to substantially increase crack growth rates while the addition of the unload/reload seemed to slow crack growth compared to the specimen statically loaded in air.
- The crystallographic plane of fracture is consistent with known hydride habit planes and the fracture surface topography is consistent facets formed in hydrogen gas atmosphere. The formation of fine tear ridges on the facet surface is consistent with localized softening due to the hydrogen enhanced localized plasticity mechanism.
- Crack propagation rates within the faceted region were on the order of 2 μm cycle^{-1} at crack lengths between 20 μm and 100 μm, considerably higher than those observed during continuous cycling. Due to the higher growth rates, cracks grew preferentially through the faceted region before extending into the adjacent, differently oriented grains. This implies that the small crack growth regime may be equally as important to explaining the 'dwell effect' as the crack initiation stage. These accelerated crack growth rates are particularly detrimental in heavily microtextured material where there is a continuous easy crack path.

Acknowledgements

This work was partially funded by the Federal Aviation Administration and the Office of Naval Research Contract No. N00014-06-1-0089. One of the authors (ALP) acknowledges support from Air Force Contract

FA8650-07-D-5800 during preparation of this manuscript. The authors are grateful to Dr. S. Fox (Timet, Henderson, Nevada) for providing the bar material used in this study and Dr. A. Bhattacharjee (Defence Metallurgical Research Lab, Hyderabad, India) for his assistance with sample preparation and measuring the texture of the as-received bar. The authors appreciate the useful discussions related to fatigue and fracture of titanium alloys with Dr. M.C. Brandes (OSU) and also J. Foltz and A. Young (OSU) for their assistance with electrical discharge machining and stress corrosion cracking experiments, respectively. Finally, the authors would also like to acknowledge Dr. E. Medina and S. Putthanarat for their assistance with non-destructive evaluations.

References

[1] L. Wagner, J.K. Gregory, A. Gysler and G. Lütjering: *in* Small fatigue cracks, Proceedings of the second engineering foundation international conference/workshop, R.O. Ritchie and J. Lankford, eds., Santa Barbera, CA, Metallurgical Society, (1986) p. 117-127.

[2] C.C. Wojcik, K.S. Chan and D.A. Koss: Stage I Fatigue Crack Propagation in a Titanium Alloy, 36;5 (1988) p. 1261-1270.

[3] F. Bridier, P. Villechaise and J. Mendez: Analysis of the different slip systems activated by tension in an α/β titanium alloy in relation with local crystallographic orientation, Acta Materialia, 53 (2005) p. 555-567.

[4] A.L. Pilchak, R.E.A. Williams and J.C. Williams, Crystallography of fatigue crack initiation and growth in fully lamellar Ti-6Al-4V, Met. Mater. Trans. A. 41A, 2010, pp. 106-124.

[5] J.E. Hack and G.R. Leverant: The influence of microstructure on the susceptibility of titanium alloys to internal hydrogen embrittlement, Metallurgical and Materials Transactions A, 13 (1982) p. 1729-1738.

[6] W.J. Evans and M.R. Bache: International Journal of Fatigue, 16;7 (1994) p. 443-452.

[7] V. Sinha, M.J. Mills and J.C. Williams: Determination of crystallographic orientation of dwell-fatigue facture facets in Ti-6242 alloy, Journal of Materials Science, 42 (2007) p. 8334-8341.

[8] V. Sinha, M.J. Mills and J.C. Williams: Crystallography of Fracture Facets in a Near-Alpha Titanium Alloy, Metallurgical and Materials Transactions A, 37;6 (2006) p. 2015-2026.

[9] M. Brandes, PhD Dissertation, The Ohio State University, 2008.

[10] J.K. Gregory and H.-G. Brokmeier. The relationship between crystallographic texture and salt water cracking susceptibility in Ti-6Al-4V. *Mat. Sci. Eng. A* (1995) vol. 203, p. 365-372.

[11] E. Richey, R. P. Gangloff, "Strain Rate Dependent Environment Assisted Cracking of alp-Ti Alloys in Chloride Solution," *Environmentally Assisted Cracking: Predictive Methods for Risk Assessment and Evaluation of Materials, Equipment, and Structures*, ASTM STP 1401, R. D. Kane, Ed., American Society for Testing and Materials, West Conshohocken, PA, (2000).

[12] W.J. Evans: Scripta Metallurgica, 21;4, 1987, pp. 469-474.

[13] M.R. Bache, H.M. Davies, W.J. Evans, in: PA Blenkinsop, WJ Evans and HM Flower, eds., Proc. of the Eighth World Conference on Titanium: Titanium ‘95, Birmingham, UK, IOM, 1996, pp. 1347-1354.

[14] M.R. Bache, W.J. Evans and H.M. Davies: Electron back scattered diffraction (EBSD) analysis of quasi-cleavage and hydrogen induced fractures under cyclic and dwell loading in titanium alloys, Journal of Materials Science, 32 (1997) p. 3435-3442.

[15] M.R. Bache: Int. J. Fatigue, 25, 2003, pp. 1079-1087.

[16] D.L. Davidson and D. Eylon: Titanium Alloy Fatigue Fracture Facet Investigation by Selected Area Electron Channeling, Metallurgical Transactions A, 11 (1980) p. 837-843.

[17] E. Uta, N. Gey, P. Bocher, M. Humbert and J. Gilgert: Journal of Microscopy, Vol. 233, Pt. 3, 2009, pp. 451-459.

[18] B. F. Brown, Fundamentals, in Stress Corrosion Cracking in High Strength Steels and in Titanium and Aluminum Alloys, BF Brown, *ed.* Naval Research Lab, Washington, DC (1972) p. 1-16

[19] D.C. Slavik, J.A. Wert and R.P. Gangloff: Determining fracture facet crystallography using backscatter patterns and quantitative tilt fractography, Journal of Materials Research, 8;10 (1993) p. 2482-2491.

[20] G. Themelis, S. Chikwembani and J. Weerman: Determination of the orientation of Cu-Bi grain boundary facets using a photogrammetric technique. *Materials Characterization*, (1990) 24, 27-40.

[21] Y.J. Ro, S.R. Agnew and R.P. Gangloff: Uncertainty in the determination of fatigue facet crystallography, Scripta Materialia,52 (2005) p. 531-536.

[22] N.E. Paton, J.C. Williams, J.C. Chesnutt and A.W. Thompson: The effect of microstructure on the fatigue and fracture of commercial titanium alloys, *in*: Alloy design for fatigue and fracture resistance. AGARD-CP-185, p. 4-1 – 4-14, London: Technical Editing and Reproduction Ltd., (1976).

[23] J.C. Chesnutt, A.W. Thompson and J.C. Williams: Influence of Metallurgical Factors on the Fatigue Crack Growth Rate in Alpha-Beta Titanium Alloys, Final Technical Report AFML-TR-78-68, (1978).

[24] R.J.H. Wanhill, R. Galatolo, C.E.W. Looije: Fractographic and microstructural analysis of fatigue crack growth in a Ti-6Al-4V fan disc forging, International Journal of Fatigue, 11;6 (1989) p. 4007-416.

[25] F. McBagonluri, E. Akpan, C. Mercer, W. Shen and W.O. Soboyejo: Trans. ASME, 127, 2005, pp. 46-57.

[26] F. McBagonluri, E. Akpan, C. Mercer, W. Shen and W.O. Soboyejo: Mat. Sci. Eng. A, 405, 2005, pp. 111-134.

[27] A.L. Pilchak, A. Bhattacharjee, A.H. Rosenberger and J.C. Williams: Int. J. of Fatigue, 31, 2009, pp. 989-994.

[28] V. Sinha, J.W. Spowart, M.J. Mills and J.C. Williams: Observations on the Faceted Initiation Site in the Dwell-Fatigue Tested Ti-6242 Alloy: Crystallographic Orientation and Size Effects, Metallurgical and Materials Transactions A, 37;5 (2006) p. 1507-1518.

[29] A.L. Pilchak, A. Bhattacharjee, R.E.A. Williams and J.C. Williams: The Effect of Microstructure on Fatigue Crack Initiation in Ti-6Al-4V, in Proceedings of the 12th International Conference on Fracture, Ottawa, Canada, 2009.

[30] A.L. Pilchak, PhD Dissertation, The Ohio State University, 2009.

[31] C.J. Szczepanski, S.K. Jha, J.M. Larsen and J.W. Jones: Metall. Mater. Trans. A, 39A, 2008, pp. 2841-2851.

[32] C.J. Szczepanski: The Role of Microstructural Variability on the Very High Cycle Fatigue Lifetime Variability of the α + β Titanium Alloy, Ti-6Al-2Sn-4Zr-6Mo, PhD Dissertation, The University of Michigan, Department of Materials Science and Engineering, 2008.

[33] J.C. Williams, R.G. Baggerly and N.E. Paton: Deformation Behavior of HCP Ti-Al Alloy Single Crystals, Metallurgical and Materials Transactions A, 33A, 2002, pp. 837-850.

[34] S. Suri, G.B. Viswanathan, T. Neeraj, D.-H. Hou and M.J. Mills: Room Temperature Deformation and Mechanisms of Slip Transmission in Oriented Single-Colony Crystals of an α/β Titanium Alloy, Acta Materialia, 47;3 (1999) p. 1019-1034.

[35] M.F. Savage, J. Tatalovich and M.J. Mills: Anisotropy in the room-temperature deformation of α-β colonies in titanium alloys: role of the α-β interface, Philosophical Magazine, 84;11 (2004) p. 1127-1154.

[36] D.L. Davidson and J. Lankford: Fatigue Crack Growth Mechanics for Ti-6Al-4V (RA) in Vacuum and Humid Air, Metallurgical Transactions A, 15 (1984) p. 1931-1940.

[37] T.L. Anderson, Fracture Mechanics: Fundamentals and Applications 3rd ed., Taylor & Francis Group, Boca Raton, FL, 2005.

[38] S. Suresh: Fatigue of Materials, 2nd ed., Cambridge University Press, New York, 1998.

[39] J.V. Bernier, J.-S. Park, A.L. Pilchak, M.G. Glavicic and M.P. Miller: Measuring Stress Distributions in Ti-6Al-4V Using Synchrotron X-Ray Diffraction, Metallurgical and Material Transactions A, 39 (2008) p. 3120-3133.

[40] X.G. Zhang, J. Vereecken, Stress Corrosion Cracking Mechanism of Ti-6Al-4V in Acidic Methanol, Corrosion. 46 (1990) 136-141.

[41] C.D. Beachem and R.M.N. Pelloux: Electron fractography – a tool for the study of micromechanisms of fracturing processes, *in* Fracture toughness testing and its applications, ASTM STP 381, (1965) p. 210-245.

[42] D.A. Meyn: Metall. Mater. Trans. A, 3A, 1972, pp. 2302-2305.

[43] C. Laird: The influence of metallurgical structure on the mechanisms of fatigue crack propagation, *ASTM STP 415*, American Society for Testing and Materials, 1966.

[44] A.P.Woodfield, M.D. Gorman, R.R.Corderman, J.A. Sutliff and B.Yamrom, Titanium 95: Science and Technology, UK, 1995, pp. 1116-1123.

[45] A.P. Woodfield, GE Aviation, private communication, 2009.

[46] V. Hasija, S. Ghosh, M.J. Mills and D.S. Joseph: Deformation and creep modeling in polycrystalline Ti-6Al alloys, Acta Materialia, 51 (2003) p. 4533-4549.

[47] G. Venkataramani, D. Deka, S. Ghosh: Crystal Plasticity Based Fe Model for Understanding Microstructural Effects on Creep and Dwell Fatigue in Ti-6242, Trans. ASME, 356;128, 2006, pp. 356-365.

[48] F.P.E. Dunne, A. Walker and D. Rugg: A systematic study of hcp crystal orientation and morphology effects in polycrystal deformation and fatigue, Proceedings of the Royal Society A, 463 (2007) p. 1467-1489.

[49] K. Kirane, S. Ghosh, M. Groeber, and A. Bhattacharjee: Journal of Engineering Materials and Technology, 131, 2009, pp. 021003-1 – 021003-14.

[50] F.P.E. Dunne and D. Rugg: Fatigue & Fracture of Engineering Materials & Structures, 31, 2008, pp. 949-958.

[51] M.C. Brandes, M.J. Mills and J.C. Williams: Metall. Mater. Trans. A, in press.

[52] J.S. Koehler, Phys. Rev. B, 85, 1952, 480-481.

[53] D.S. Shih, I.M. Robertson and H.K. Birnbaum, Acta. Metall., 36, 1988, pp. 111-124.

[54] P.E. Irving and C.J. Beevers, Some Metallographic and Lattice Parameter Observations on Titanium Hydride, Metall. Mater. Trans. A., 1971, pp. 613-615.

[55] J. C. Williams: *in* Effect of Hydrogen on Behavior of Materials, A.W. Thompson and I. M. Bernstein, eds., AIME, NY, 1976, p 367-381.

[56] J.D. Boyd: Trans. ASM, 62, 1969, p. 977-88.

[57] A.R. Troiano: Trans. ASM, 1960, vol. 52., pp. 54-80.

[58] I.M. Robertson and H.K. Birnbaum: Dislocation mobility and hydrogen – a brief review, *in*. Proc. 11th International Conference on Fracture, http://www.icf11.com/proceeding/EXTENDED/5759.pdf, accessed 19 Dec 2009.

[59] N.E. Paton and R.A. Spurling: Metall. Mater. Trans. A, 7A, 1969, pp. 1769-1774.

[60] M.I. Luppo, A. Politi, and G. Vigna: Acta Mater., 53, 2005, pp. 4987-4996.

[61] X.H. Guo, S.Q. Shi, Q.M. Zhang, and X.Q. Ma: J. Nucl. Mater., 378, 2008, pp. 110-119.

[62] M.R. Louthan: Trans. Metall. Soc. AIME, 227, 1963, pp. 1166-1170.

[63] M.R. Louthan, R.P. Marshall: J. Nucl. Mater. 9, 1963, pp. 170-184.

[64] R.N. Singh, R. Kishore, S.S. Singh, T.K. Sinha, B.P. Kashyap, J. Nucl. Mater. 325, 2004, pp. 26-33.

[65] A.R. Massih and L.O. Jernkvist, Computational Mater. Sci. 46 (2009) pp. 1091-1097.

[66] M.-S. Yeh and J.-H. Huang, Mat. Sci. Eng. A 242, 1998, p. 96-107.

[67] R.H. Rusli, Mat. Sci. Eng. A 494, 2008, p. 143-146.

[68] A.W. Bowen: Influence of Crystallographic Orientation on Fatigue Crack Growth in Strongly Textured Ti-6Al-4, Acta Metallurgica, 23;11 (1975) p. 1401-1409.

[69] W.J. Evans and C.R. Gostelow, Metall. Mater. Trans. A. 10;12, 1979, pp. 1837-1846.

[70] J.C. Chesnutt and N.E. Paton, in: Titanium '80: Science and Technology, Proc. 4th World. Conf. on Titanium, Kyoto, Japan, 1980, pp. 1855-1863.

[71] A.W. Sommer and D. Eylon: Metall. Mater. Trans. A, 14;10, 1983, pp. 2178-2181.

[72] W. Shen, A.B.O. Soboyejo, and W.O. Syejo, Metall. Mater. Trans. A, 35(1), 2004, pp. 163-187.

[73] W. Shen, W.O. Soboyejo, and A.B.O. Soboyejo: Mechanics of Materials, 36(1-2), 2004, pp. 117-140.

[74] A.A. Shaniavski and A.I. Losev: Fatigue and Fracture of Engineering Materials and Structures, 26(4), 2003, pp. 329-342.

[75] L. Toubal, P. Bocher, A. Moreau: Int. J. Fatigue, 31, 2009, pp. 601-605.

[76] A. Bhattacharjee, D.M. Norfleet, M.J. Mills and J.C. Williams, unpublished research, The Ohio State University, 2006 and 2009.

[77] V. Sinha, R.B. Schwarz, M.J. Mills and J.C. Williams, unpublished research, The Ohio State University, 2004.

List of figures and figure captions.

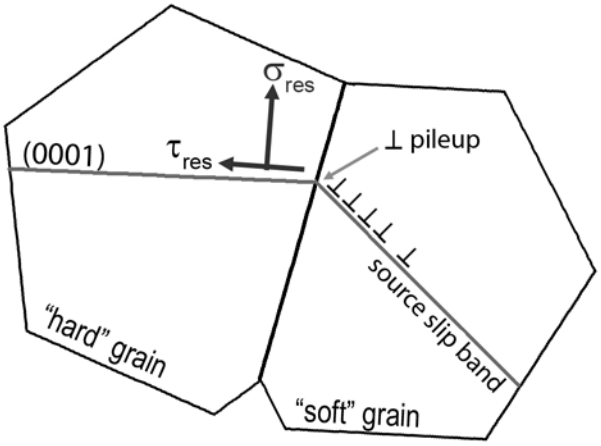

Figure 1. Schematic representation of the Stroh model as modified by Evans and Bache [6] for dwell fatigue.

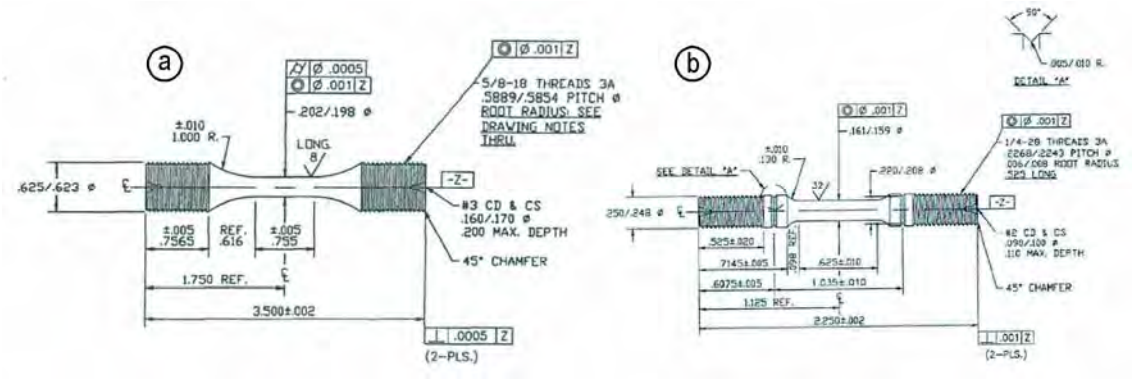

Figure 2. Specimen drawings for (a) cyclic and dwell tests and (b) static loading tests.

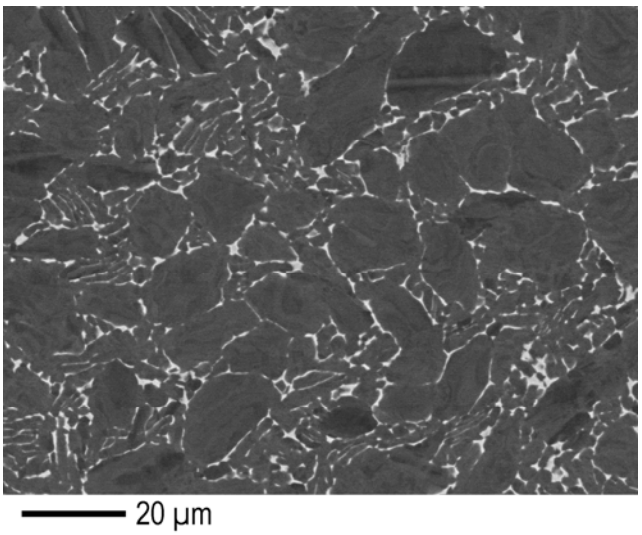

Figure 3. Microstructure of the as received Ti-811 bar.

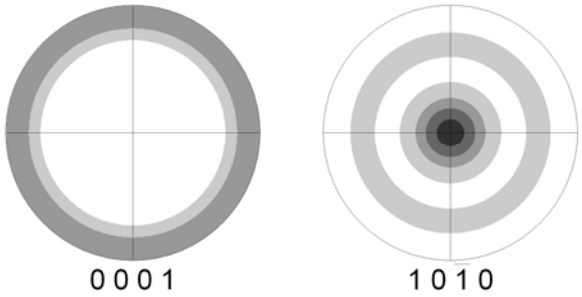

Figure 4. The texture of the as-received bar calculated from large area EBSD scans. A weak $10\bar{1}0$ partial fiber is present along the bar axis which is perpendicular to plane of projection. The levels of intensity are in intervals of 0.5 multiples of the probability of a random distribution.

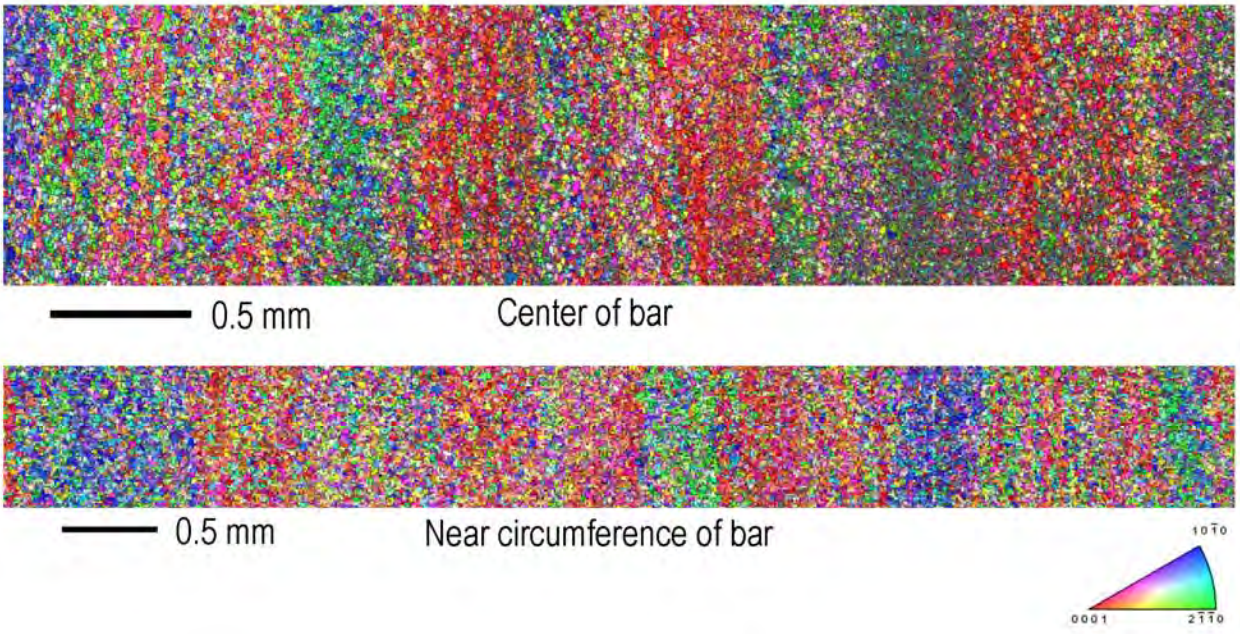

Figure 5. Normal direction inverse pole figure EBSD maps of longitudinal sections of the bar cut from near the center and edge showing elongated bands of microtexture. The loading direction is perpendicular to the plane of polish

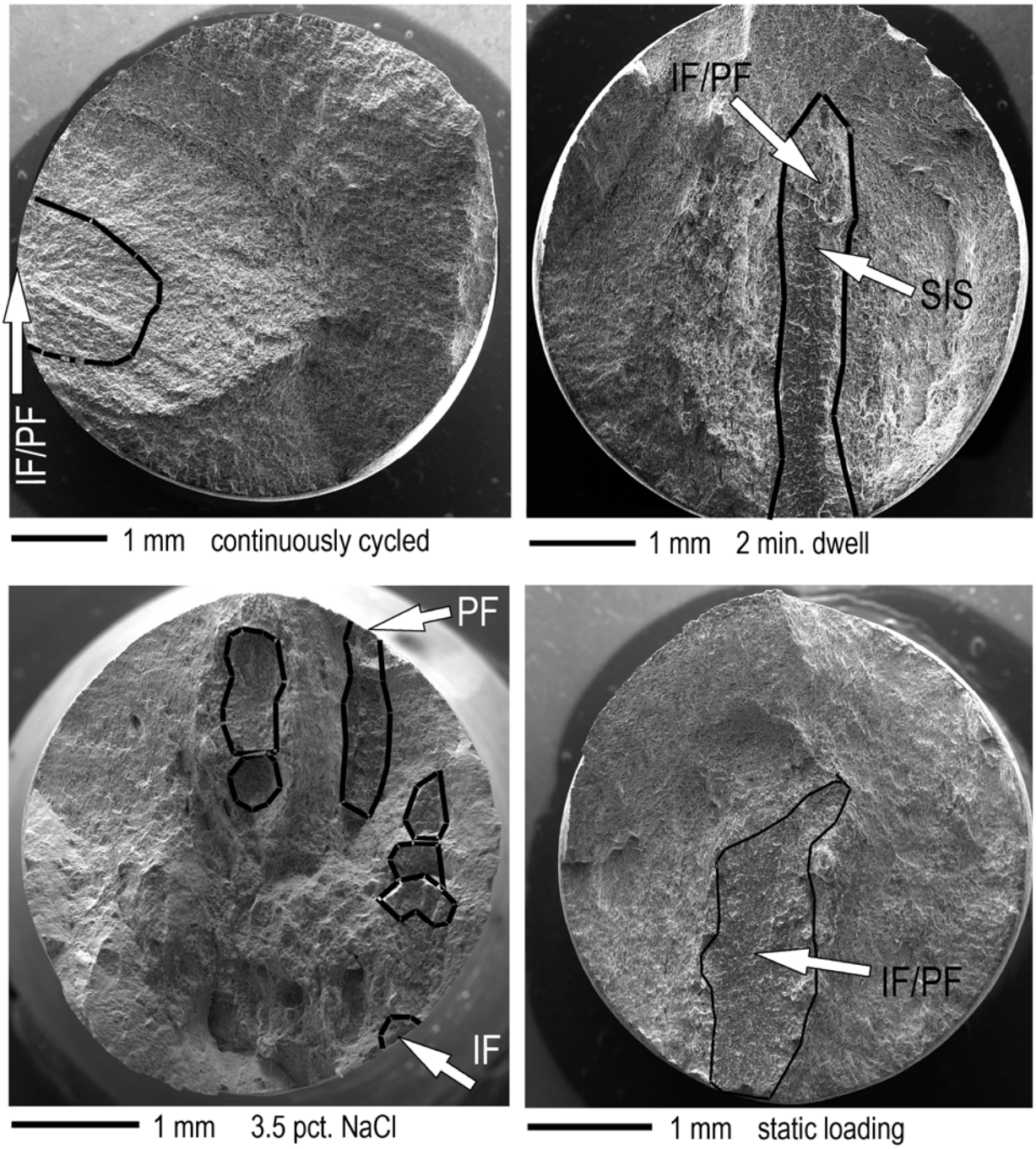

Figure 6. Low magnification SEM images of the fractured specimens. The faceted regions on each specimen are enclosed by black lines. The locations of the initiation facets (IF) and propagation facets (PF) discussed in more detail below are identified on each fracture surface. The location of a secondary initiation site (SIS) on the dwell fatigue specimen is also shown.

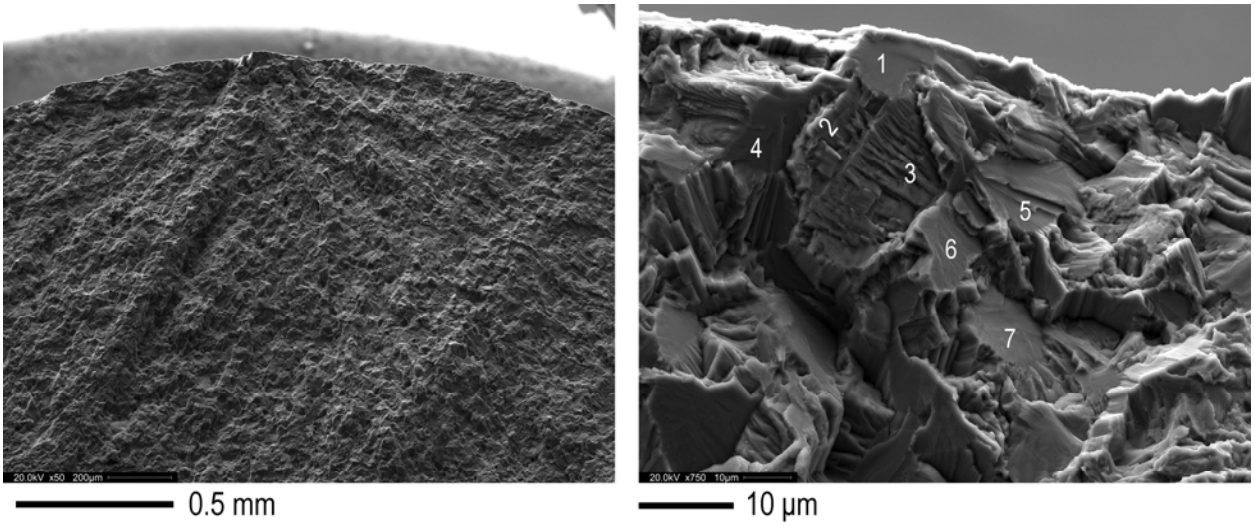

Figure 7. Crack initiation site in the continuously cycled specimen in the as-received condition. Several facets are identified by the integers 1 through 7. The number, N, corresponds to the last digit in the facet serial number H2-1-N.

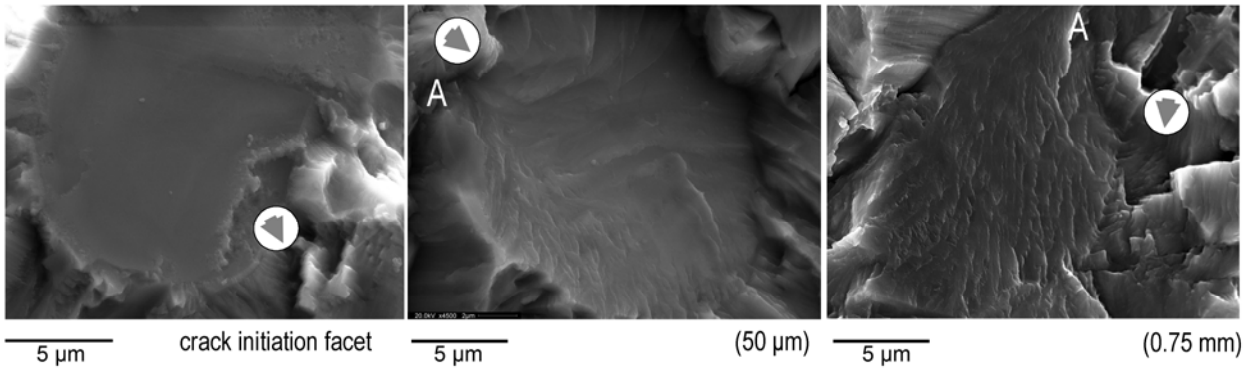

Figure 8. The effect of crack length on facet topography in the cyclically loaded specimen in the as-received condition. The local crack propagation direction is indicated by the arrows while the letter A designates the point at which the crack entered the grain.

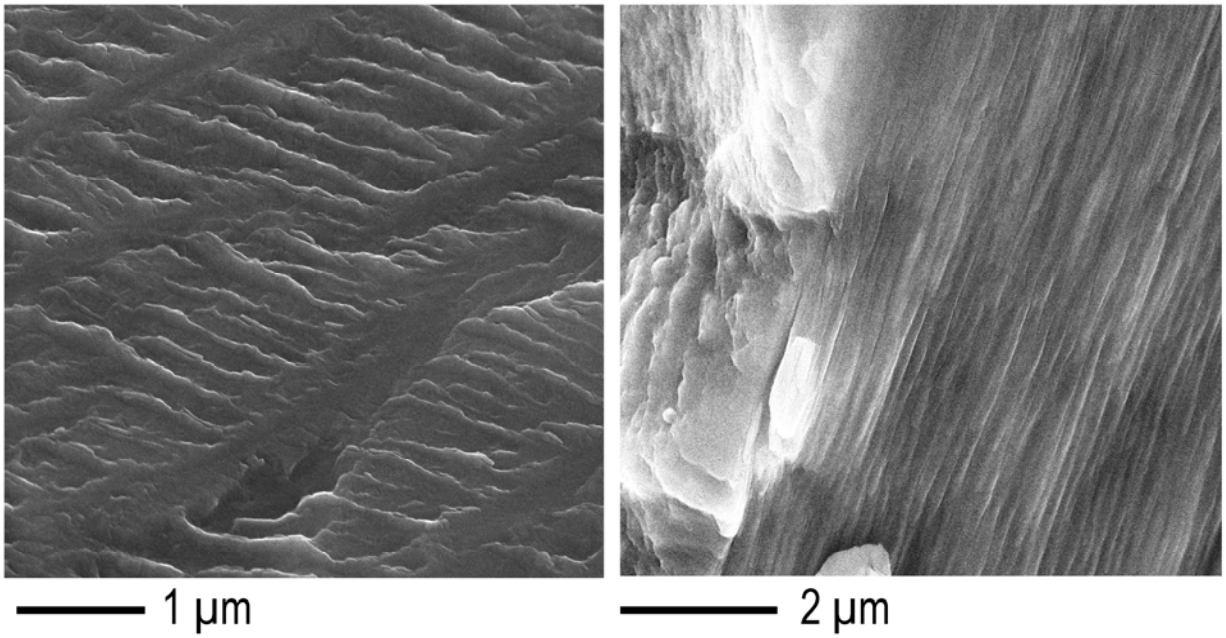

Figure 9. High magnification secondary electron images of two different facet surfaces in the continuously cycled specimen at crack lengths ~100 µm. The markings on the facet surfaces suggest the crack growth growth rate is on the order of 150 nm / cycle.

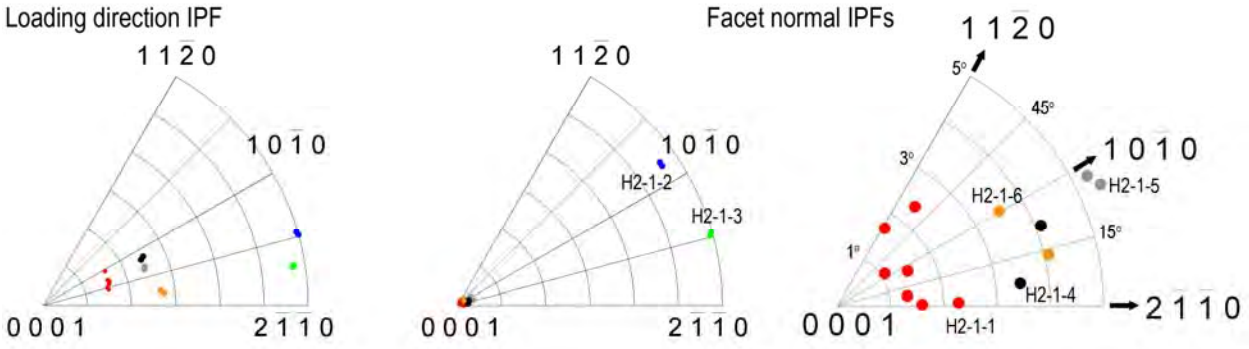

Figure 10. Results from the facet crystallography analysis on the continuously cycled fatigue specimen. The IPF on the right is a magnified view of the region around 0001 in the center facet normal IPF (also note the change in scale for this IPF).

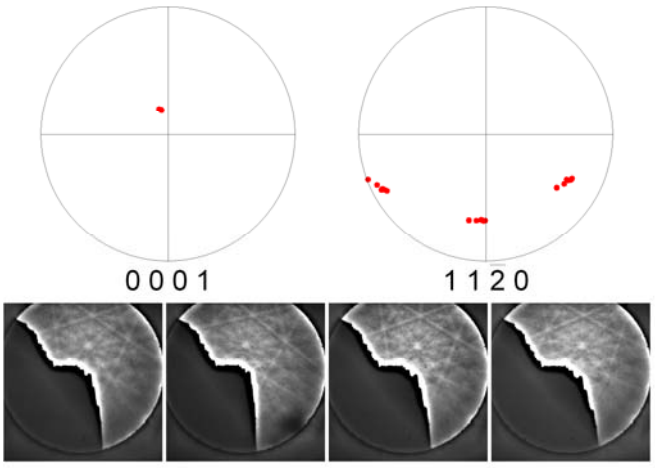

Figure 11. 0001 and $11\bar{2}0$ pole figures showing all of the orientations indexed from the crack initiation facet (H2-1-1) in the continuously cycled specimen. The basal pole remains in the same position, however there is a rotation of 10° about [0001] over a distance of approximately 7 μm on the facet. Four of the seven total EBSD patterns are shown to provide an indication of pattern quality. Although part of the detector is shadowed by other parts on the fracture surface, there are sufficient zone axes present to make an accurate determination of the crystallographic orientation with a high degree of confidence.

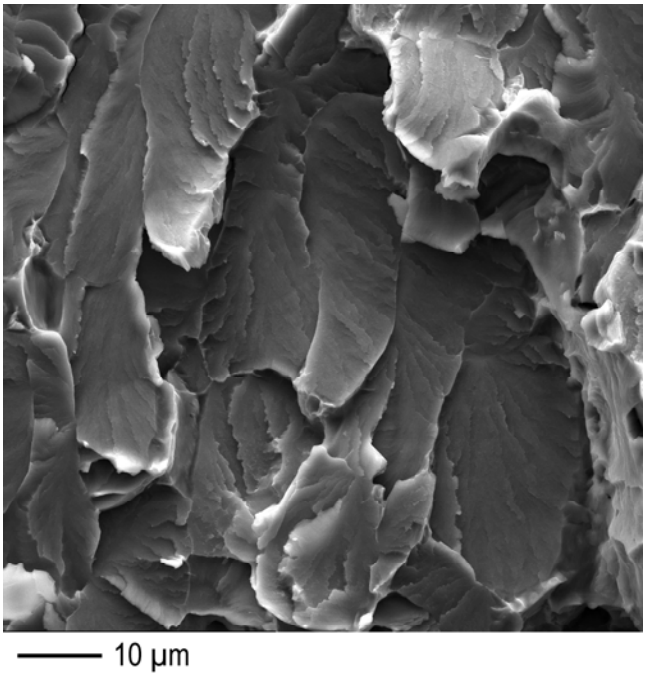

Figure 12. Typical facet appearance throughout the entire faceted region on the specimen statically loaded in air.

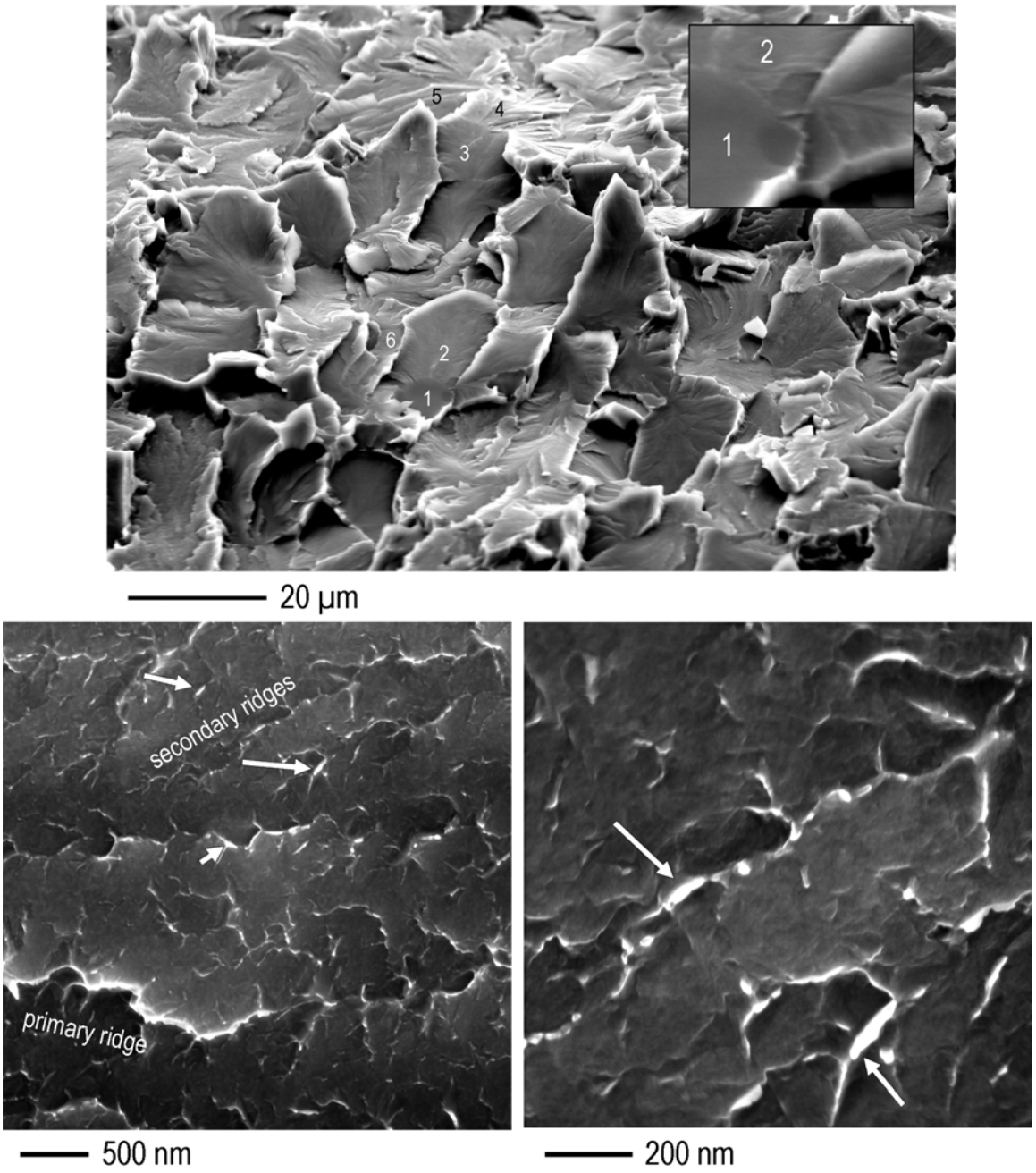

Figure 13. (Top) Secondary electron image of a crack initiation site in the statically loaded specimen (H3-4). Six facets are identified which were analyzed in detail. The initiation site is shown at higher magnification in the inset. (Bottom) High resolution images showing the facet topography of typical crack propagation facets. The macroscopic crack propagation direction is from left to right. See text for information regarding arrows.

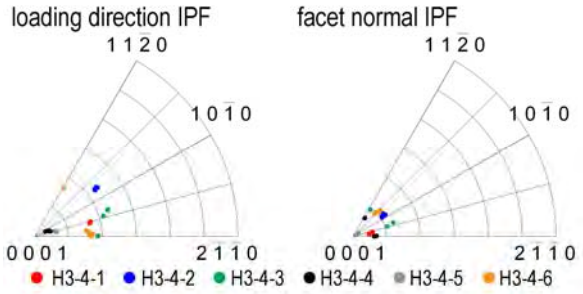

Figure 14. Results from the facet crystallography analysis on the initiation (H3-4-1) and propagation (all others) facets from the statically loaded specimen

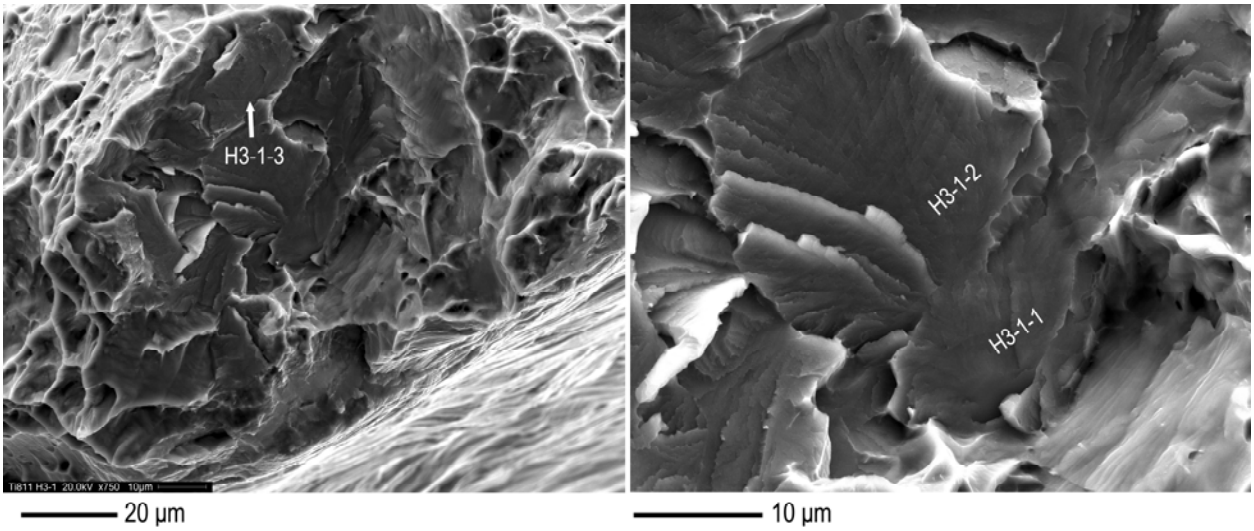

Figure 15. The facets nearest to the surface of the sample on the as-received specimen subjected to static loading in 3.5 pct. NaCl at 95 pct. of the yield strength.

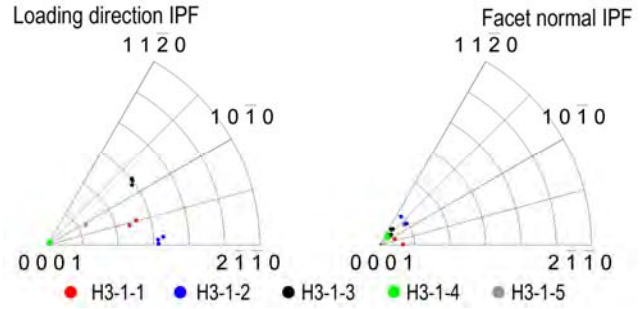

Figure 16. Initiation and propagation facet crystallography for the as-received SCC specimen. Facets H3-1-4 and H3-1-5 are propagation facets while the others are the near-initiation site facets.

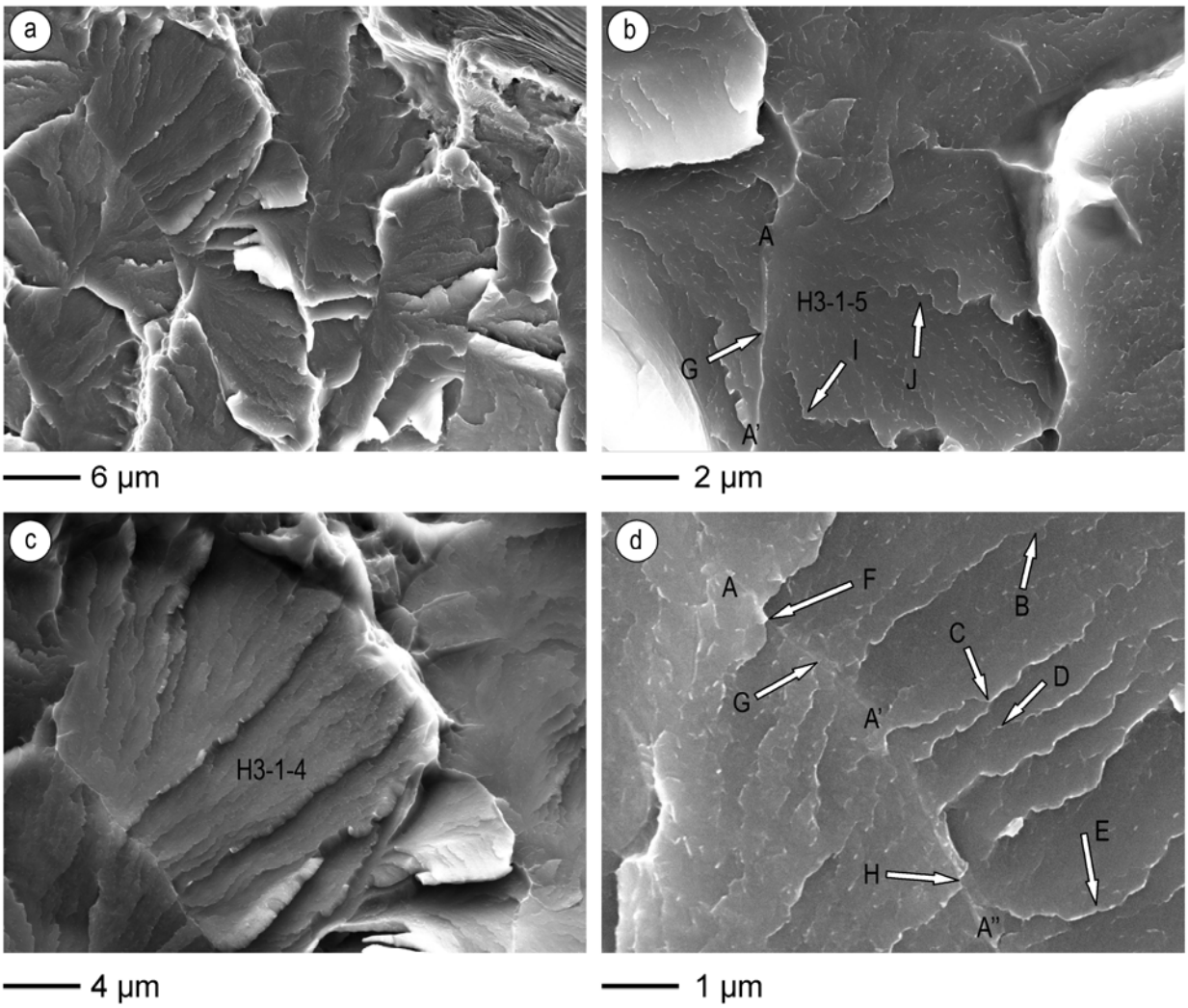

Figure 17. Propagation facets on the fracture surface of the as-received specimen subjected to static loading in 3.5 pct. NaCl at 95 pct. of the yield strength. Those facets analyzed in detail have been labeled with unique facet identification numbers. See text for details regarding the features identified by letters in (d).

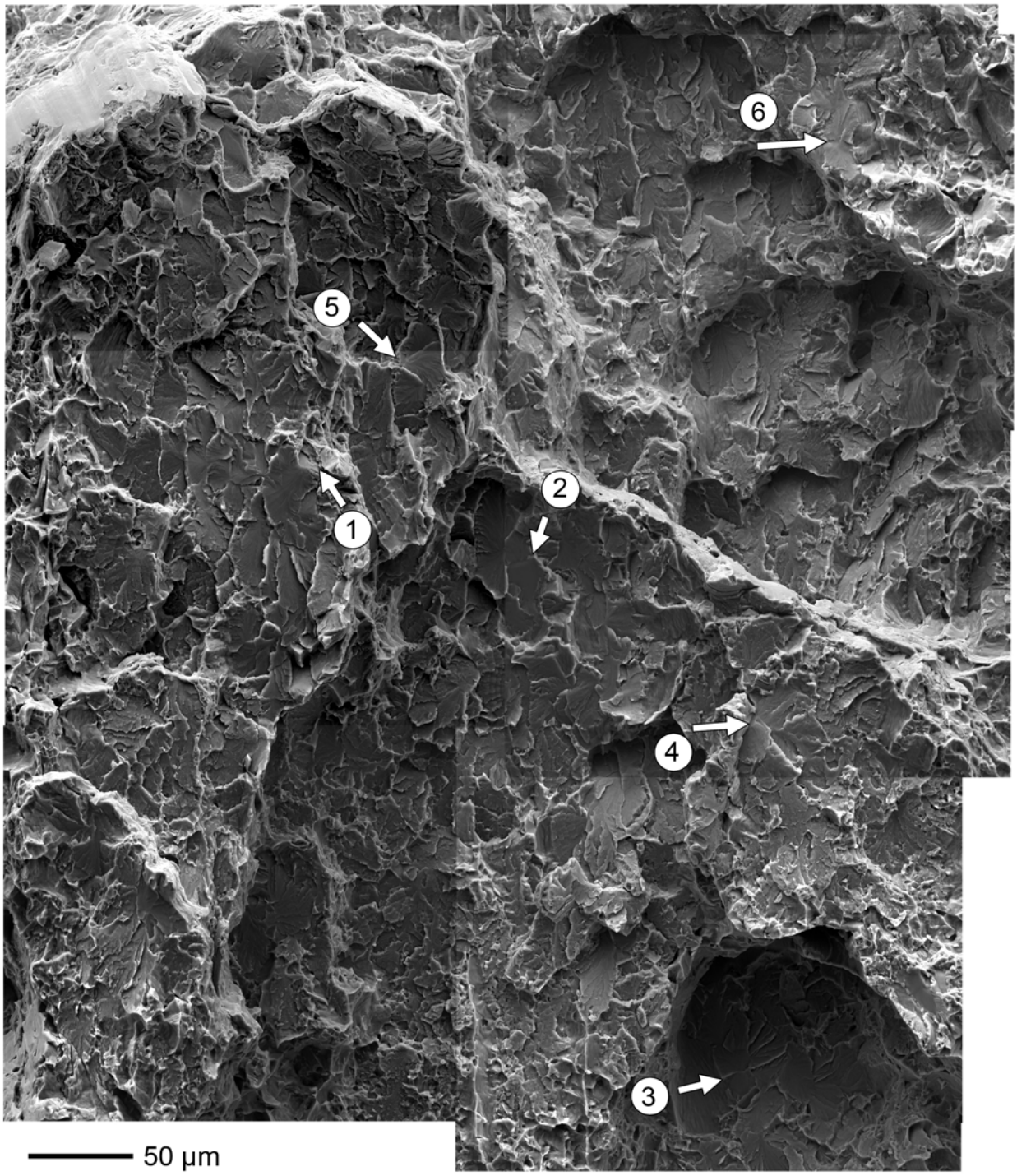

Figure 18. Higher magnification secondary electron montage of the region around the primary initiation site (1) which reveals several secondary initiation sites (2-6).

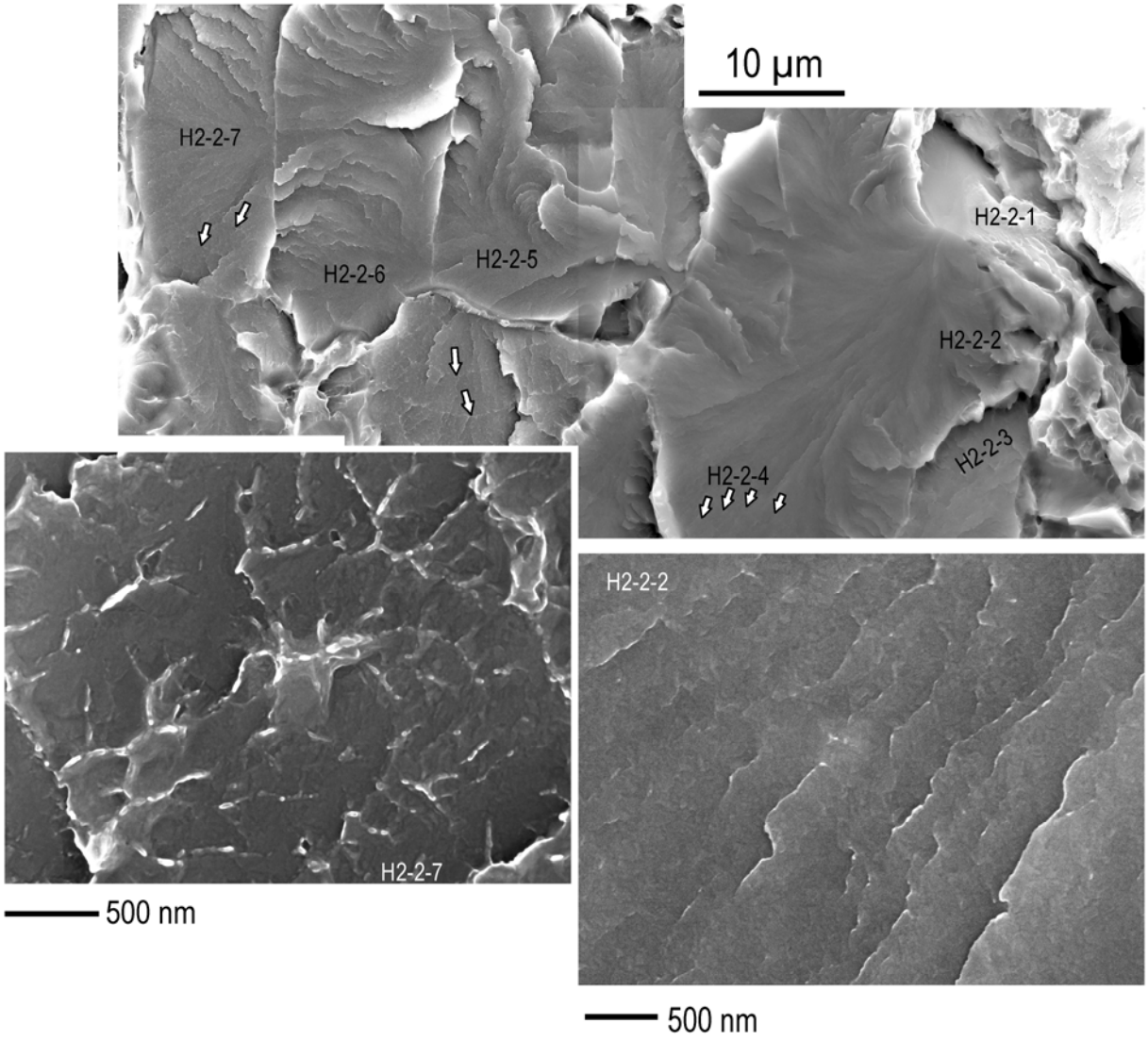

Figure 19. High resolution secondary electron images of the fracture surface of the dwell fatigue specimen (all at 0 deg. stage tilt). The top image shows the initiation facet (H2-2-1) which is inclined substantially to the loading axis and subsequent propagation facets (H2-2-2 through H2-2-7). The arrows in the top image identify crack front arrest marks.

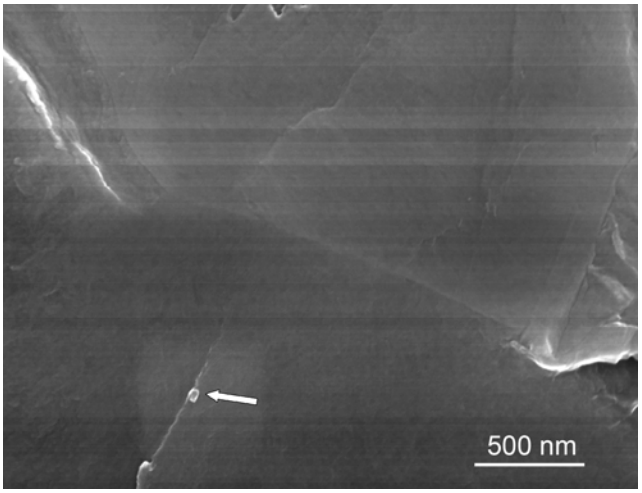

Figure 20. The intersection of facets H2-2-1 and H2-2-2 at the primary dwell fatigue crack initiation site. The arrow identifies a small particle near the first ridge formed on the first propagation facet. The composition and crystallographic structure of this feature is unknown.

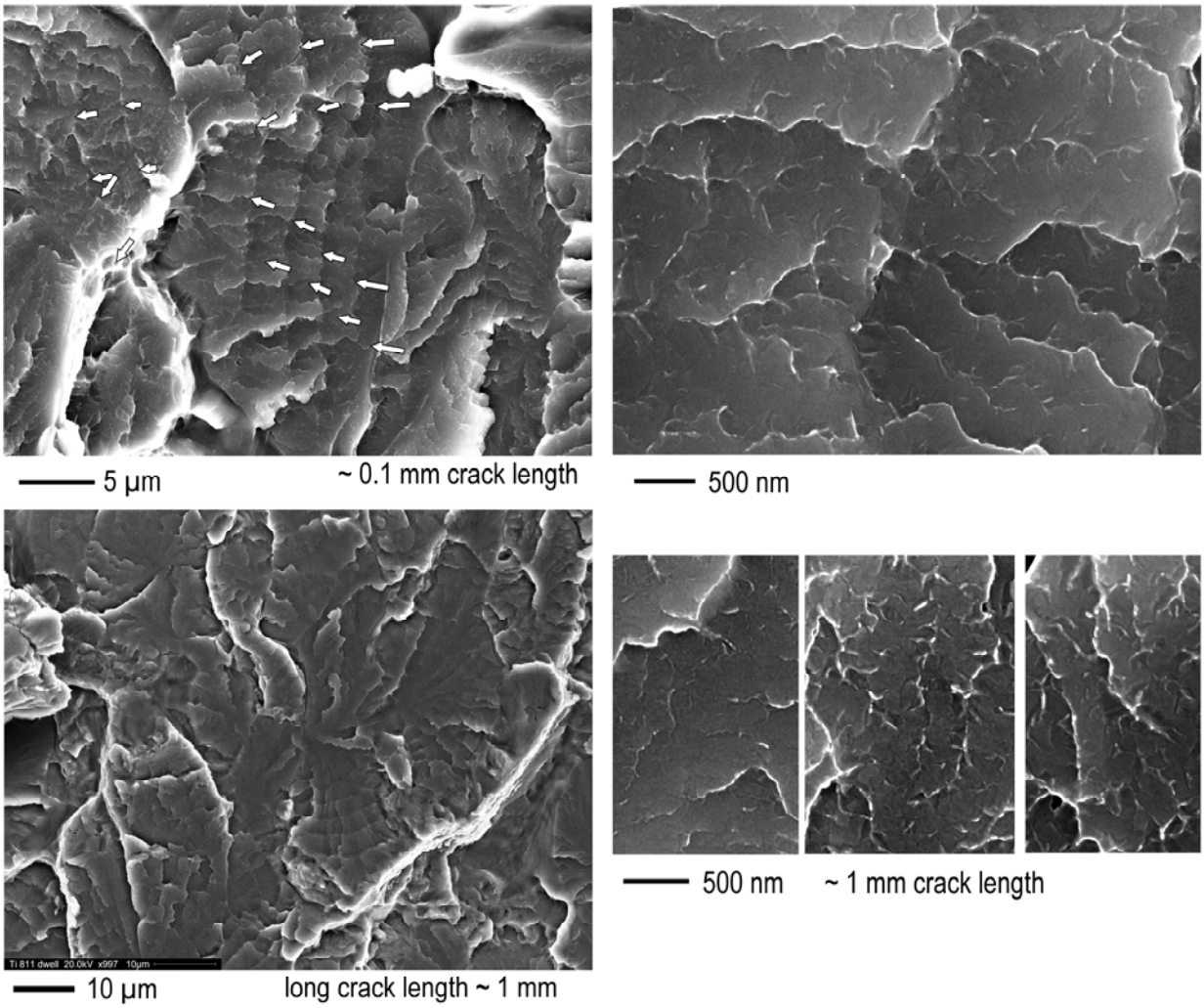

Figure 21. Secondary electron images showing very little variation among the facet surface topography as a function of crack length in the dwell fatigued specimen. A secondary initiation site is also evident in the center of the lower left image.

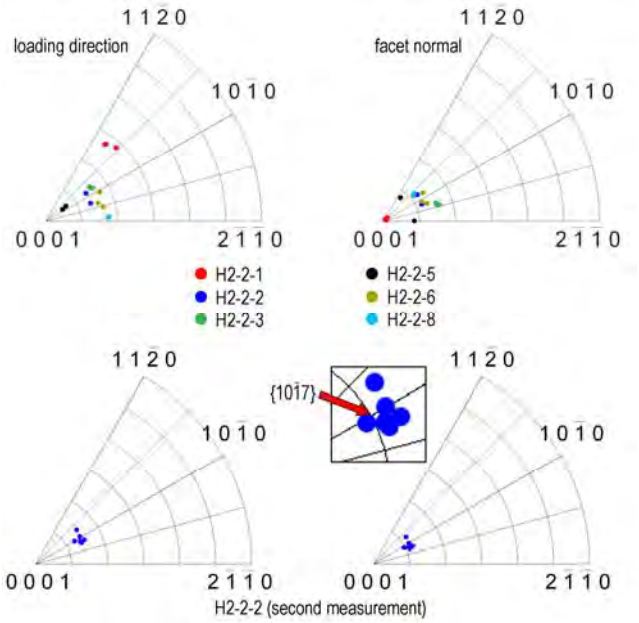

Figure 22. Dwell fatigue facet crystallography. Equal angle inverse pole figures showing the orientations of the faceted grains identified in Figure 19 with respect to the loading direction and facet normal.

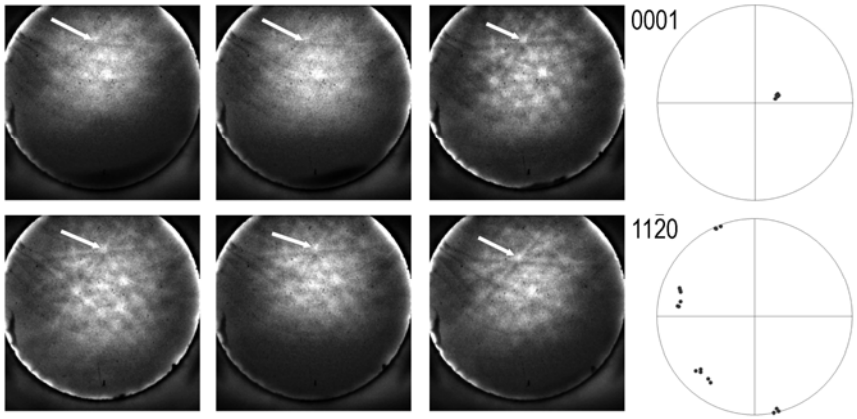

Figure 23. EBSD patterns collected from the as-fractured H2-2-2 facet during the second analysis at locations successively further from the initiation site. The white arrows identify the [1$\bar{2}$13] zone axis, which shifted subtly, in each pattern. The indexed orientations are represented on the 0001 and 11$\bar{2}$0 pole figures and reveal a ~10^{o} rotation about [0001].

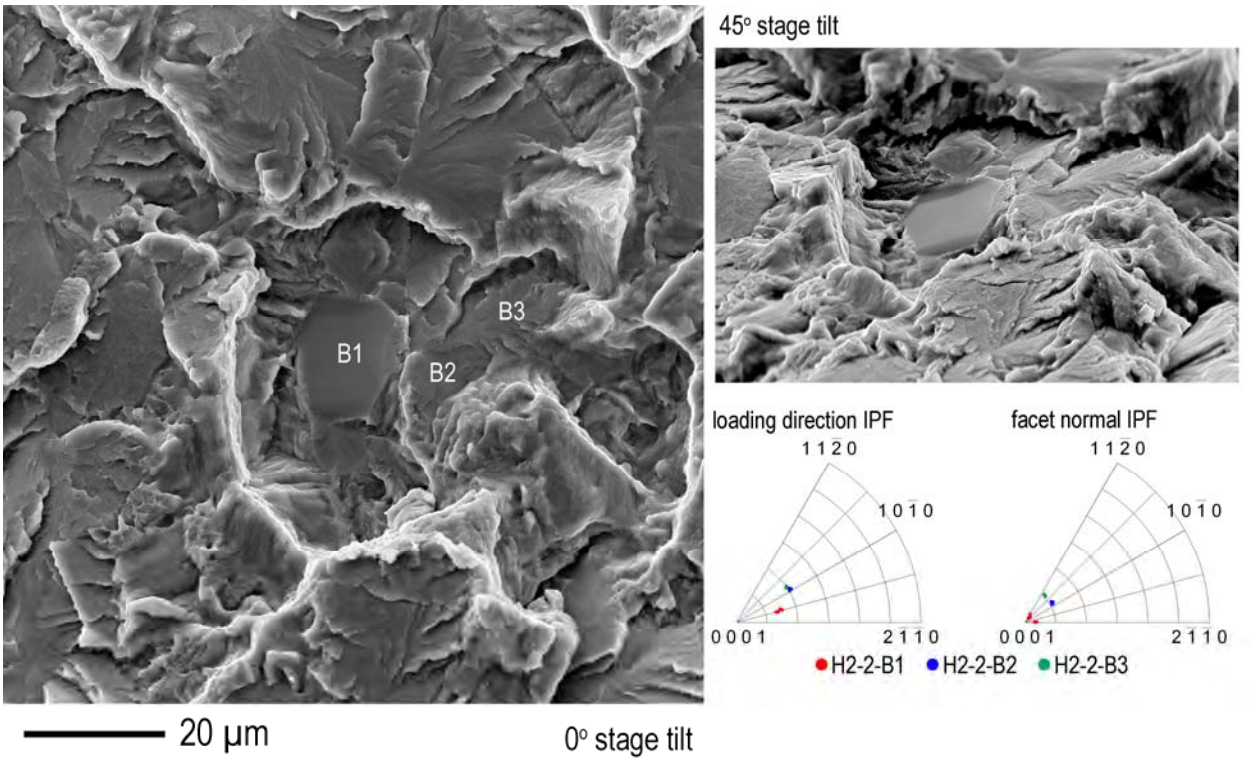

Figure 24. Secondary electron images and facet crsytallography analysis of a secondary initiation site in the dwell fatigued specimen. This location is approximately 380 µm away from the primary initiation site.

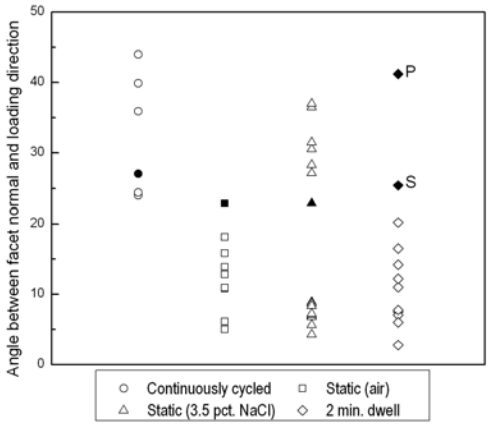

Figure 25. Angle between facet normal and loading direction. Filled symbols indicate initiation facets while open symbols designate propagation facets. Letters P and S designate the primary and secondary initiation sites studied on the dwell specimen.

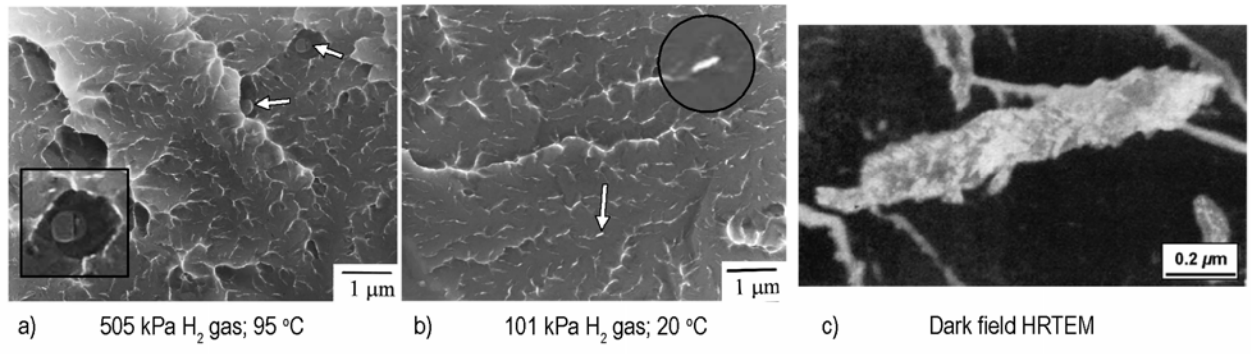

Figure 26. (a) and (b) Surface topography of facets formed by static loading in Ti-6Al-4V alloy in H_2 gas [66]. The arrows in (a) point to features that are presumably plate-like TiH_2 precipitates, the top of which is shown at higher magnification in the 1 μm wide inset. Smaller, bright particles similar to those observed on the Ti-811 facets in the present study were also observed. One is identified by the arrow in (b) and also shown at higher magnification in the 0.5 μm diameter inset. (c) A dark field TEM image of a precipitate like the one identified in (b), except in the alloy Ti-8Al-1Mo-2V, lifted from the fracture surface in an acetate replica [67].

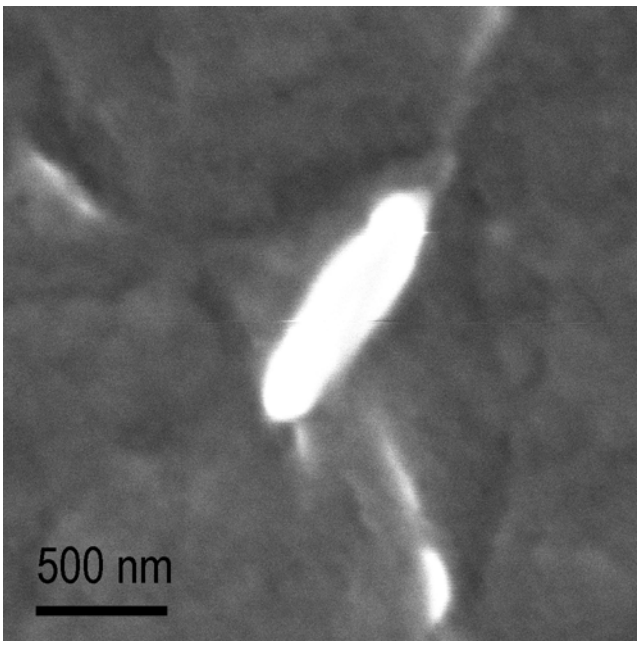

Figure 27. Secondary electron image (TLD detector, 256,000x) of a possible hydride particle from a dwell fatigue propagation facet.

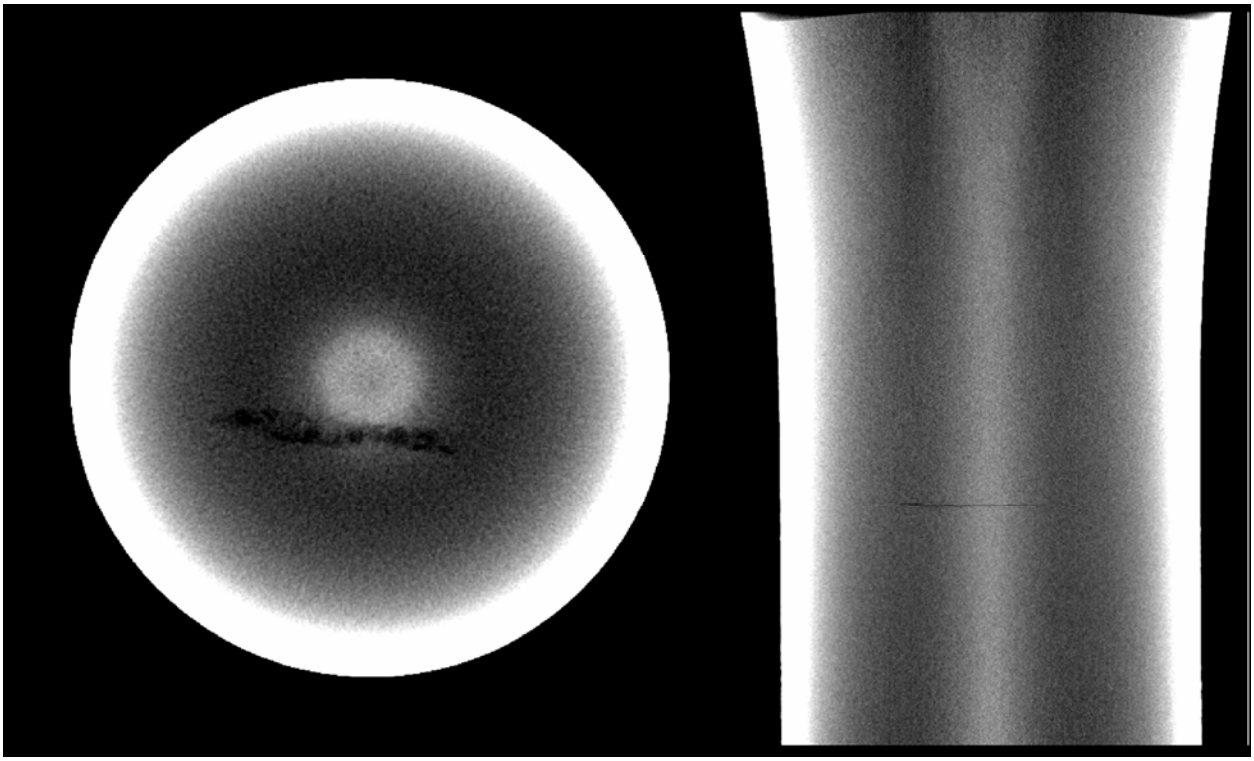

Figure 28. Two orthogonal view of an x-ray computed tomography scan of a dwell specimen which had not failed after 26k cycles.

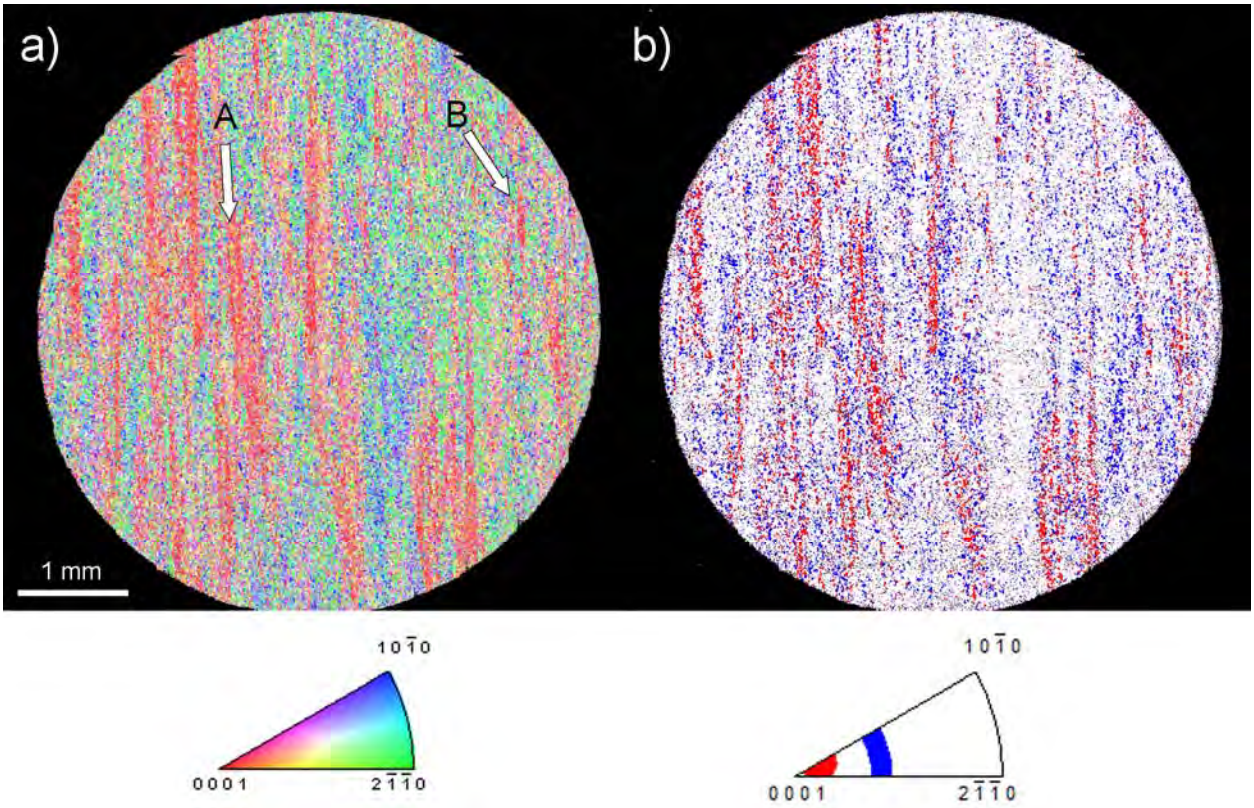

Figure 29. (a) Loading direction inverse pole figure map of a transverse cross section of the dwell fatigue specimen approximately 1.3 mm beneath the fracture surface. In (b), those grains with basal poles inclined 40° to 50° from the loading direction have been colored blue while the red grains are those with a $\{10\bar{1}7\}$ plane that is no more than 10° away from being orthogonal to the loading direction, as indicated by the inverse pole figures beneath each diagram. See text for details regarding locations A and B in (a).